Modeling halotropism: A key role for root tip architecture and reflux loop remodeling in redistributing auxin

Thea van den Berg[1,#], Ruud A. Korver[2,#], Christa S. Testerink[2], Kirsten H.W.J. ten Tusscher[1]

[#]**these authors contributed equally**

[1]Theoretical Biology, Department of Biology, Utrecht University, The Netherlands

[2]Plant Cell Biology, Swammerdam Institute for Life Sciences, University of Amsterdam, The Netherlands

summary statement:

Halotropism allows plant roots to bend away from salt. We use a computational model to disentangle how observed changes in auxin transport generate the auxin assymetry necessary for root bending. Predictions generated by the model were experimentally validated.

corresponding author:

Kirsten ten Tusscher, email k.h.w.j.tentusscher@uu.nl

keywords:

plant development, root tropism, auxin transport, modeling, computer simulation

Abstract

A key characteristic of plant development is its plasticity in response to various and dynamically changing environmental conditions. Tropisms contribute to this flexibity by allowing plant organs to grow from or towards environmental cues. Halotropism is a recently described tropism allowing plant roots to bend away from salt. During halotropism, as in most other tropisms, directional growth is generated through an asymmetric auxin distribution that generates differences in growth rate and hence induces bending. Here we develop a detailed model of auxin transport in the Arabidopsis root tip and combine this with experiments to investigate the processes generating auxin asymmetry during halotropism. Our model points to the key role of root tip architecture in allowing the decrease in PIN2 at the salt-exposed side of the root to result in a rerouting of auxin to the opposite side. In addition, our model demonstrates how feedback of auxin on the auxin transporter AUX1 amplifies this auxin asymmetry, while a salt-induced transient increase in PIN1 levels increases the speed at which this occurs. Using AUX1-GFP imaging and pin1 mutants we experimentally confirmed these model predictions, thus expanding our knowledge of the cellular basis of halotropism.

Introduction

Plant development is characterised by a large degree of flexibility, termed developmental or phenotypic plasticity. Due to their sessile nature, plants have very limited influence over the environmental conditions they find themselves in. As a consequence, plants had to evolve the capacity to survive in different environments as well as dynamically changing environmental conditions by making their developmental programs dependent on environmental signals. The resulting phenotypic plasticity enables plants to flexibly adjust to their environmental conditions. This developmental plasticity may influence overall architecture, for example the layout of the root system, by influencing meristem size and hence the rate of root growth [Aquea et al., 2012, Chapman et al., 2011, Jain et al., 2007, Liu et al., 2015,West et al., 2004] as well as the number of developing or outgrowing lateral roots [Jain et al., 2007]. Another, perhaps more subtle, adaptation of plant development involves the directional growth of plant organs towards or away from a perceived stimulus, such as the gravity vector [Abas et al., 2006,Sukumar et al., 2009], light [Wan et al., 2012,Laxmi et al., 2008,Sassi et al., 2012] or nutrients [Niu et al., 2015]. Recently, we described a new tropism, called halotropism that entails the directional growth of plant roots away from salt [Galvan-Ampudia et al., 2013].

At the base of most plant tropisms lies an asymmetric distribution of the plant hormone auxin [Went, 1974] that generates asymmetric growth rates and thus causes bending. Auxin patterns are strongly determined by auxin transport. Auxin can enter cells both via passive diffusion as well as active transport mediated via the AUX/LAX family of importers [Rutschow et al., 2014, Swarup et al., 2008, Benett et al., 1996]. Auxin importers have a tissue specific expression pattern [Benett et al., 1996, Péret et al., 2012, Swarup et al., 2001, Swarup et al., 2005], leading to the preferential retention of auxin in particular tissues. Auxin can only leave cells via active transport, dominated by the PIN family of exporters [Friml et al., 2003,Petrasek et al., 2006, Wisniewska et al.,

2006,Paponov et al., 2005]. In addition to having tissue specific expression domains, PIN proteins have a tissue and PIN type specific polar membrane pattern, leading to directional auxin transport fluxes [Friml et al., 2002a,Friml et al., 2003,Benková et al., 2003]. In plant roots a reverse fountain PIN pattern generates a symmetrical auxin gradient with a maximum close to the root tip [Blilou et al., 2005, Grieneisen et al., 2007]. During root tropisms, bending is caused by an asymmetric elevation of auxin in the expansion zone that causes an asymmetric repression of expansion rates [Scheitz et al., 2013,Thimann, 1936].

The best studied tropism in plant roots is gravitropism. Upon a gravitropic stimulus, columella cell statoliths sediment onto the downward oriented membrane face [Eshel and Beeckman, 2013]. Via an as of yet unidentified mechanism this causes the polarisation of the normally apolar PIN3 and PIN7 proteins onto the downward membrane [Friml et al., 2002b]. As a consequence, most auxin arriving in the root tip now becomes transported towards the downward side. The auxin dependence of PIN2 membrane levels [Chen et al., 1998, Abas et al., 2006] and AUX1 gene expression levels [Laskowski et al., 2006, Laskowski et al., 2008] enable these transporters to amplify this initial auxin asymmetry and transport part of the excess auxin towards the expansion zone where it can affect expansion rates and induce root bending [Chen et al., 1998,Abas et al., 2006,Luschnig et al., 1998,Müller et al., 1998,Benett et al., 1996,Swarup et al., 2001]. Thus, while PIN3 and PIN7 appear to have a primary, asymmetry inducing role, PIN2 and AUX1 appear to have a secondary, amplifying and transducing role [Eshel and Beeckman, 2013].

Intriguingly, we reported in an earlier study that the salt induced auxin asymmetry causing halotropic root bending co-occurred with a reduction of epidermal PIN2 at the salt-exposed side of the root. No asymmetries in other PINs were reported. These data imply that PIN2, which has a mostly secondary role in gravitropism [Abas et al., 2006,Wan et al., 2012,Kleine-Vehn et al.,

2008], plays a primary, asymmetry generating role in halotropism. The gravitropism induced polarity switch in PIN3 and PIN7 in the root tip, where all auxin fluxes converge, biases auxin transport in one direction. This causes an auxin increase at one side of the root and an auxin decrease at the opposite side as two sides of the same coin. In contrast, although it can be easily understood that the halotropism induced reduction of epidermal PIN2 will lead to a decrease of auxin at the salt exposed side, it is far less trivial to see how this should lead to a concomittant increase in auxin at the opposite side. As a consequence, currently two alternative scenarios remain possible. In the first, PIN2 is the sole auxin asymmetry generator, and the reduced transport of auxin at one side of the reflux loop somehow leads to a translocation of this auxin towards the opposite side of the reflux loop. Alternatively, another not yet identified auxin asymmetry generating source may be present under halotropism.

In the current study we use a detailed model of auxin transport in the Arabidopsis root tip to investigate whether the measured changes in PIN2 are necessary and sufficient to explain the auxin asymmetries observed under halotropism. We combine our modeling with experiments aimed at unraveling the potential role of salt induced changes in other PINs in generating or amplifying auxin asymmetry, as well as to confirm predictions generated by our model. Our computer simulations reveal the critical importance of taking into account a realistic wedge-shaped root tip architecture for studying root tropisms. In absence of this realistic architecture, a PIN2 reduction at the salt exposed side fails to induce any auxin increase at the opposite side, while in its presence a modest auxin increase is automatically induced. We show that this increase was enhanced substantially when taking into account the auxin dependence of AUX1 [Benett et al., 1996] and PIN2 [Paciorek et al., 2005, Whitford et al., 2012, Baster et al., 2012]. Furthermore, our model predicts that underlying this enhanced auxin asymmetry is an asymmetry in AUX1 and PIN2

patterns. We experimentally validate this prediction for AUX1, demonstrating that exposure to a salt gradient results in an elevation of AUX1 levels on the non-salt exposed versus salt-exposed side. In addition, we experimentally demonstrate that exposure to a salt gradient induces a transient, symmetric upregulation of PIN1. Incorporating this in our model significantly amplifies the auxin asymmetry arising in the early phases of halotropism, thus speeding up the halotropic response. Finally, we experimentally validated this role of PIN1 in root halotropism, by showing that pin1 mutants exhibit a delayed halotropic response.

Our study suggests that the observed changes in PIN2 are responsible for the primary generation of auxin asymmetry. This asymmetry is subsequently further enhanced by the feedback of auxin on PIN2 itself and AUX1, and effectively sped up by a transient upregulation of PIN1. Together this provides the necessary and sufficient conditions for generating an auxin asymmetry capable of inducing effective root bending.

Results

Halotropic auxin asymmetry

To be able to judge whether the auxin asymmetries occurring in our simulations are sufficient to explain halotropic root bending, we first need to establish the amount of auxin asymmetry actually occurring during halotropism. For root tropisms it is well known that auxin elevation leads to repression of cell expansion rates [Mullen et al., 1998,Band et al., 2012]. However, it is less clear whether the concomittant decrease in auxin at the opposite side of the root contributes to growth rate asymmetry and bending by stimulating growth rate. Thus, we take a conservative approach, assuming that tropic bending is only caused by auxin elevation and growth inhibition.

In an earlier study [Galvan-Ampudia et al., 2013] we quantified the changes in DR5 and DII-Venus auxin reporter under halotropism. A~0.8 fold change in DR5 and ~1.2 fold change in DII-Venus was found at the salt-exposed side, and a ~1.2 fold change in DR5 and ~0.9 fold decrease in DII-Venus at the non-salt exposed side. In an earlier study by Band et al. it was shown that during gravitropism a ~0.7 fold change in DII-Venus occurred on the lower side of the root and that this corresponds to an approximately 2 fold increase in auxin levels [Band et al., 2012]. Extrapolating these data, it was approximated that the change in DII-Venus observed during halotropism corresponds to a ~1.3–1.4 fold increase in auxin levels.

Root tip architecture

The key question of this study is whether and how a reduction of epidermal PIN2 at the salt-stressed side can cause a rerouting of auxin to the non-salt exposed side of the root. We hypothesize that root tip architecture plays a key role in this proces. To investigate this we developed three alternative root tip architectures. In the first, the baseline model, a highly simplified rectangular representation was used, similar to previous studies [Grieneisen et al., 2007, Laskowski et al., 2008, Mironova et al., 2010, Tian et al., 2014,Mähönen et al.,

2014] (Fig. 1A1). In the second, extended model, a realistic-wedge shaped root tip architecture containing root cap tissue was applied (Fig. 1A2). This architecture somewhat resembles the root tip model used in Cruz-Ramirez et al. [Cruz-Ramírez et al., 2012]. Differences are the more narrow root tip architecture, the stronger curvature and resulting smaller left-right distances close to the root tip, and the decrease in number of vascular cell files close to the root tip in our model, that we believe more realistically represents Arabidopsis root tip topology. The third architecture (Fig. 1A3) is a variant of the second, in which vascular cells and outer columella cells are increased in width. It should be noted that during root ageing typically all tissues increase in width [Zhu et al., 1998]. We are not modeling root ageing here. Rather, we increased the width of only the internal tissues to specifically investigate the impact of left-right distances between epidermal and lateral root cap tissues for auxin rerouting. For further details we refer to the Materials and Methods section.

Note that while in the baseline model only vascular tissue connects directly to the QC and epidermal, cortical and endodermal cell files end on the columella, in the extended model these tissues all end in a curvature directly on or near the QC. Furthermore, in the extended model the columella tiers are directly connected to either the epidermis or the lateral root cap. Since these tissues have a predominantly upward PIN pattern all columella tiers are thus connected to shootward transporting tissue files. In contrast, in the baseline model columella cells are connected both to upward transporting epidermal and downward transporting cortical and endodermal tissue. These differences can be expected to subtly affect properties of the auxin reflux loop. Indeed, in Fig. 1B it can be observed that in the extended model auxin levels are reduced in the columella, and elevated in the epidermal and outer vascular cell files as compared to the baseline model.

Salt-induced changes in PIN2

To monitor salt-gradient induced auxin rerouting we plot percentage change in epidermal auxin levels (Fig. 2A), overall root pattern of auxin levels (Fig. 2B) and auxin rerouting (Fig. 2C). In the latter, we measure in each root cell whether auxin levels are elevated by at least 1% in case of the rectangular root topology, or at least 10% in case of the wedge shaped root topology.We record the earliest timepoint at which such an elevation occurs and depicting this time with a colour code, thus generating a map of temporal auxin rerouting.

Halotropism simulations were started by applying a 20% reduction of apical PIN2 levels in epidermal cells on the salt stressed side of the baseline root model. In Fig. 2A1 and 2B1 we see that this results in an asymmetric distribution of auxin. However, in contrast to experimental results where auxin decreases at the salt stressed side and increases at the non salt stressed side, auxin decreases at both sides of the root. In Figure 2C1 mapping auxin rerouting we see that halotropism results in a fast increase of auxin levels in the lowermost regions of the salt-exposed side. Clearly, the PIN2 reduction at the salt-exposed side results in a “traffic jam” leading to auxin accumulation upstream of the transport blockage. No rerouting of auxin to the non-salt-exposed side occurs. Instead, the lower auxin levels at the non-exposed side imply that a reduction of overall reflux loop efficiency has occurred. Next, the same salt stress scenario was applied to our model extended with a realistic root tip architecture. Now one can observe that besides a decrease of auxin at the salt stressed side auxin increases -albeit to a minor extent- at the non stressed side (Fig. 2A2). Besides its modified root tip shape the extended model also contains root cap tissue. The rootcap has a similar PIN2 expression as the epidermis. It is therefore likely that the root cap PINs are similarly affected by salt stress. When root cap stress is added to the model, the auxin increase at the non stressed side is augmented (Fig. 2A2). Internalization of PIN2 from the apical membrane can hypothetically lead to elevated deposition of PIN2 on the lateral membrane.

Indeed, our earlier data suggested a small increase in localization of PIN2 on the lateral inward membrane of cells at the salt-stressed side of the root [20]. Addition of this lateral upregulation in the extended model increases the auxin asymmetry (Fig. 2A2, 2B2), this was also the case when instead of a lateral a basal upregulation of PIN2 was added (data not shown). However when this same increase in lateral PIN2 was added to the baseline, rectangular root model, the decrease in auxin on the non-salt exposed side was even more severe (Fig. 2A1). Thus, while lateral PINs potentiate the translocation of auxin from the stressed to the non stressed side in the realistic root tip architecture, in a rectangular root tip architecture this merely further cripples the effectiveness of the reflux loop.

Looking at the auxin rerouting map (Fig 2C2) for the wedge-shaped root, we observe a moderate rerouting of auxin to the lowermost parts of the non-salt-exposed side. Note however that for the wedge shaped root a threshold of 10% auxin increase is used for mapping auxin rerouting, while we used a 1% threshold value in the baseline square root model. Applying this lower threshold value in the wedge shaped root model would reveal that auxin rerouting extends more shootward, consistent with the small increase in epidermal auxin levels seen in Figure 2A2 (Fig S1). The increase in auxin levels at the non-salt-exposed side of the root involves an initial rerouting against the normal direction of auxin transport as dictated by the polar PIN pattern of the reflux loop (Figure 1A). This rerouting arises from auxin accumulating due to lack of upward oriented PIN2 transport, thereby increasing auxin uptake by the cells below it, now also causing accumulation in this cell, thus leading to the backward propagation of accumulated auxin. Only once the midline of the root is passed this accumulated auxin can join the normal direction of transport at the opposite non-salt-exposed side of the root. Our results suggest that a more realistic wedge-shaped root tip is essential for at least some of the accumulated auxin to reach this midline and become rerouted to the non-exposed side.

We hypothesized that the potential to reroute auxin to the non-exposed side critically depends on the shorter distance between left and right epidermis (and lateral root cap) tissue in the extended model compared to the baseline model. To test this we use a variant of the extended model in which the root tip still has a wedge shape and contains a lateral root cap but these distances have been increased (Fig. 1A3). Fig. 2A2 shows how this results in a reduction of the auxin increase at the non-salt exposed side of the root, thus confirming our hypothesis.

Note that the maximum observed increase in auxin levels at the non-stressed side of the root are 12-14% (extended model, salt-stress induced decrease of apical and increase of lateral PIN2 levels). This is substantially less than the auxin increase observed during halotropism experiments.

AUX/LAX-pattern and auxin feedback on it's expression

Until now influx of auxin from the walls into the cell was assumed equal for all cells. However, active import of auxin occurs by AUX/LAX membrane proteins which exhibit a tissue specific expression pattern [Benett et al., 1996, Swarup et al., 2001, Swarup et al., 2005, Péret et al., 2012]. In gravitropism AUX1 is essential for the adequate propagation of the initial auxin asymmetry [Benett et al., 1996, Swarup et al., 2001]. Therefore we decided to investigate the potential role of AUX/LAX importers in halotropism. Focusing on the changes in auxin levels in the elongation zone of the root ($\geq 500 \mu m$ from root tip) incorporation of the AUX/LAX tissue specific expression results in an increase of auxin levels on both sides of the root (Fig. 3A). This logically follows from the preferred retention of auxin in AUX/LAX expressing cells, such as the epidermis. Overall auxin asymmetry actually decreased as a result of AUX/LAX incorporation into our model. However, the expression of auxin importers is known to be positively regulated by auxin [Laskowski et al., 2006,Laskowski et al., 2008]. This auxin dependence may allow AUX/LAX importers to respond to and amplify auxin asymmetry. Earlier studies have

demonstrated the patterning potential of auxin feeding back on its own transporters [Galvan-Ampudia et al., 2013]. Addition of this auxin dependence indeed led to an increase in asymmetry, specifically the non-stressed side increased in auxin level (Fig. 3A), resulting from a substantially increased rerouting of auxin to this side (compare Figures 2C2 and 3B). Indeed, auxin levels at the non-salt exposed side now increased by ~30%, which is close to the factor 1.3-1.4 increase we estimated to occur during halotropic root bending. Another difference is that compared to Figs 1B2 and 2B2, the auxin pattern in Figure 3B more closely resembles experimentally measured patterns with low auxin levels in meristematic epidermal cells, and epidermal auxin levels increasing above the end of the root cap where the elongation zone starts [Brunoud et al., 2012,Band et al., 2014] (see also Fig. S2). Clearly, incorporating realistic AUX/LAX patterns is crucial for correctly simulating auxin patterns. Underlying the enhanced halotropic auxin asymmetry, we see that AUX/LAX expression decreased on the salt-exposed side and increased on the non-exposed side (Fig. 3B). This asymmetry in AUX/LAX expression in not restricted to the epidermis, as the auxin importers are also asymmetrically expressed in the vasculature (Fig. 3B). This vascular asymmetry is consistent with the observed asymmetry in auxin signalling in the vasculature in halotropism experiments [Galvan-Ampudia et al., 2013].

Next, we set out to experimentally validate the asymmetry in AUX/LAX pattern predicted by our model, focusing on AUX1 as the major auxin importer involved in tropisms. We measured AUX1 membrane patterns, assuming that AUX1 membrane occupancy is linearly related to AUX1 expression levels, as is the case in our model. Figure 3C shows an AUX1 pattern in a control root, which is expected to have a symmetric AUX1 pattern. Note the apparent asymmetry in vascular AUX1 patterns, which is due to the protophloem cells not always lying symmetrically in the focal plane. While this is something that can be avoided in many studies, this is not the case in our study where we do

not want to interfere with root orientation relative to the salt gradient. For these reasons, we focus on epidermal AUX1 patterns for which both sides are clearly visible (Fig 3C). As can be seen in Figure 3B our model predicts AUX1 patterns to be symmetric close to the root tip, and start diverging shootward from the rootcap. To test for such a spatial pattern we measured AUX1 levels in the epidermal outer membranes, allowing us to measure the longitudinal AUX1 pattern starting from the rootcap and going shootwards, and determine the development of left right differences along this axis by computing ratios between non-exposed and salt-exposed sides (Fig. 3D). Consistent with our model predictions, close to the root cap salt-exposed roots show an approximately symmetric AUX1 pattern comparable to that of control roots (ratio close to 1), while higher upward asymmetry builds up with the non-exposed side having larger AUX1 levels than the salt-exposed side (ratio close to 1.45). We tested for statistical significance of these findings by binning AUX1 ratios in 5000 micron spanning length segments for both salt-exposed and control roots, using a double sided T-test to test per segment whether AUX1 ratios differ significantly. All segments were found to differ significantly (Supplementary table 1).

Auxin feedback on PIN2 membrane levels

PIN proteins are constitutively cycling between the membrane and cytoplasmic vesicles.Experiments suggest that auxin may reduce the internalization of PINs, which would allow it to enhance its own export from the cell [Paciorek et al., 2005]. However, effects are significantly stronger for synthetic than naturally occurring auxins [Paciorek et al., 2005, Rakusová et al., 2011]. On the other hand, more indirect interactions involving SCF(TIR1/AFB)-auxin signalling and GOLVEN peptides, also appear to cause auxin dependent regulation of PIN2 membrane levels [Baster et al., 2012, Whitford et al., 2012]. When this feedback is added on top of the AUX/LAX pattern and feedback, the asymmetry in auxin is increased, especially in the

lower part of the elongation zone, while auxin asymmetry in higher parts of the root decreased (Fig. S3A). Note that the concurrent asymmetry in PIN pattern underlying this (change in) auxin asymmetry is considerably smaller than the one observed for AUX/LAX, but again shows a decrease in the salt-exposed side and an increase on the non-exposed side(Fig. S3B) (for more details see Supplementary Results).

Salt-induced upregulation of PIN1

In an earlier study we performed a control experiment aimed at verifying whether applied salt concentrations would affect internalization of other PINs besides PIN2, cellular PIN1, PIN2, and PIN3 levels were determined under uniform salt exposure [Galvan-Ampudia et al., 2013]. Intriguingly, PIN1 and PIN3 were found to be significantly upregulated by salt. Since these PIN1 and PIN3 elevations were observed under uniform high-level salt exposure and measured at a single time point we now investigated to what extent physiologically relevant changes in PIN1 and PIN3 membrane levels occur in response to a salt gradient over the course of time (Fig. 4A, Fig S4).

We find that, consistent with the earlier observed increase in cellular PIN1 levels, PIN1 membrane levels increase by ~22% (Fig4.A left 3 images, Fig S4A). However, the increase in PIN1 levels is transient. After 2 hours of exposure PIN1 membrane levels have returned to their normal non-salt stressed levels (Fig. 4A, S4A). No indications for differences in PIN1 upregulation between the salt-exposed and non-exposed side of the root were found. Strikingly, in contrast to the earlier observed large increase in cellular PIN3 levels, PIN3 membrane levels show only a 4% transient upregulation (Fig. 4A right 3 images, Fig S4B). The observed salt-induced changes in PIN1 and PIN3 protein levels were similar for different membrane compartments as well as the intracellular compartment (Fig. S4), indicating that changes are not caused by changes in membrane cycling dynamics. The difference in findings between current and earlier experiments is likely caused by the much higher

concentration of salt applied when dipping the roots in uniform salt concentration, as compared to the more subtle treatment of growing seedlings on a salt gradient (for a more extensive discussion see Supplementary Results).

Returning to our computational model, we investigated how the transient increases in PIN1 and PIN3 could contribute to generated auxin asymmetry. First the influence of a 1.3 fold PIN1 and 1.1 fold PIN3 elevation were investigated in isolation, ignoring for a moment auxin feedback on auxin transporters and the transient nature of the PIN1 and PIN3 elevations. It can be seen that the PIN1 elevation significantly enhances auxin asymmetry, in particular by elevating auxin at the non-salt exposed side (Fig. 4B) In contrast, the small PIN3 elevation has no observable effect on auxin asymmetry. Therefore, we restrict our further analysis to the PIN1 elevation. Next we added the transient nature of the PIN1 increase to the model, both in isolation and in a setting incorporating the feedback of auxin on auxin transporters. In Fig. 4C we plotted the changes in epidermal auxin levels at the start of the elongation zone ($590\mu m$ from the root tip) as a function of time. Interestingly, we see an elevated auxin asymmetry relative to control conditions during the transient PIN1 elevation in absence of feedback (Fig. 4C red versus blue lines), indicating that symmetric PIN1 elevation contributes to asymmetry generation. This increased asymmetry gradually disappears once PIN1 has returned to normal levels (Fig. 4C), indicating that a transient PIN1 increase has no persistent effect on auxin asymmetry. If we combine the transient PIN1 elevation with feedback on auxin transporters we see that PIN1 increase causes an asymmetry that is slightly larger than the one generated by feedback alone (compare orange and green lines), and that in presence of feedback the PIN1 induced asymmetry decreases more slowly (compare orange and red lines). Most importantly the transient PIN1 increase enhances the auxin asymmetry present during the first hours of halotropism (compare speed of auxin rerouting Figs 3B and 4D). In addition to speeding up the buildup of auxin asymmetry, a transient PIN1 elevation also

causes an overshoot in auxin asymmetry levels during the early phases of halotropism. This agrees with our our earlier observation that auxin asymmetry is higher after 4 than after 6 hours of salt exposure [Galvan-Ampudia et al., 2013].

To test the experimentally predicted importance of PIN1 we tested halotropic responses on a salt gradient over a 48h timecourse in plants homozygous for the pin1 tDNA insertion compared to plants having a single or double copy of the wildtype PIN1 allele. In Figure 4E-F we show the angle from gravity 24h and 48h after exposure to a 125mM or 200mM salt gradient or control conditions. For the 24h time point we see that for both salt concentrations plant homozygous for the pin1 tDNA insertion showed a significantly smaller angle from gravity relative to both heterozygote plants and plants homozygous for the wildtype allele, indicative of a reduction of halotropic response strength in absence of PIN1. After 48h of exposure to a salt gradient the homozygous pin1 tDNA plants showed similar angles. This demonstrates that PIN1 conveys only a transient increase in halotropic response strength that is no longer present at 48h, consistent with our model predictions (for an explanation of why halotropic angles remain constant (125mM) or even decrease (200mM) from 24 to 48h we refer to the Supplementary Results).

Robustness of the results

In complex models such as these, testing the robustness of simulation outcome to specific model settings is of paramount importance to determine whether a general mechanism rather than an obscure, rare outcome has been found.

To investigate the dependence on particular model assumptions, we varied a model assumption influencing the location of the main source of auxin in our model which might potentially affect auxin patterns and fluxes and hence auxin asymmetry generated under halotropism. In the current model all root cells have a small potential to produce auxin, and a major source of auxin is

provided by influx from the shoot. However, recent data indicate that localised, root tip auxin production plays a major role in shaping the root's auxin pattern [Ljung et al., 2005, Stepanova et al., 2008]. Therefore, as an alternative, we performed simulations in which shoot to root auxin flux was reduced by a factor 2, while auxin production was elevated by a factor 100 in the QC and in root cap cells auxin production was increased by a factor 50 while decay was decreased by a factor 2. Parameter settings were chosen such that for ease of comparison similar overall auxin content was achieved. Fig. S5 shows that this change in model setup results in a highly similar auxin asymmetry pattern as compared to the default model settings. Thus, a shift in main auxin source from the shoot-root connection to the root tip does not impact our model outcome.

Next, to investigate the robustness of model outcome to parameter values we varied most of our model parameters over a range of a factor 0.5 to 1.5 of their original values. In Figure S6 we show the outcomes of our robustness analysis. We see that for all parameters tested limited quantitative variations in obtained auxin asymmetry occur for changes in parameter values, while maintaining qualitatively similar results. Based on these results we conclude that model outcomes depend to a limited extent and in a smooth, linear fashion on parameter settings, thus implying robustness of our model outcomes.

Discussion

We recently described halotropism as a new directional response of plants roots allowing them to grow away from salt [Galvan-Ampudia et al., 2013]. In the current study we used a detailed model of plant root auxin transport to investigate whether our earlier observations can account for halotropc root bending.

Our simulation study points to the critical role of root tip architecture. We find that in a simplified rectangular root model, a reduction of PIN2 on the salt exposed side merely results in the accumulation of auxin in the meristem. In contrast,in a realistic, wedge-shaped tip architecture the PIN2 decrease generates a small increase in auxin at the opposite root side. We showed that this potential to reroute auxin from the salt-exposed to the non-exposed side depends positively on the presence of a lateral root cap, the increase of lateral PINs on the salt-exposed side, and a limited distance between epidermis and root cap of salt-exposed and non-exposed side. Together this indicates that the potential for lateral transport of the auxin accumulating at the salt-exposed side is of critical importance. In addition we demonstrated an important role for positive feedback of auxin on its own transporters. Auxin induced upregulation of AUX/LAX importers substantially elevated the auxin asymmetry generated by root tip architecture. The predicted asymmetry in AUX1 pattern resulting from this feedback was confirmed experimentally. Finally, we demonstrated that PIN1 is transiently upregulated under a salt gradient. While this transient PIN1 change has no effect on long term auxin asymmetry, it significantly enhances auxin asymmetry levels during the early stages of salt stress. We speculate that generating auxin elevation at a faster rate is important to ensure root bending away from the salt before the tip of the root has started to grow into the salt contaminated area. We experimentally validated these predicted roles of AUX1 and PIN1 in halotropism.

In conclusion, our study shows that a decrease in PIN2 on the salt

exposed side can function as the primary generator of auxin asymmetry, but is not enough to generate a sufficiently large auxin asymmetry sufficiently fast. For this, the feedback of auxin on its own transporters and the transient salt-induced upregulation of PIN1 play a critical role. Interestingly, in gravitropism the pin3 mutant is not agravitropic [Kleine-Vehn et al., 2010], starch mutants remain partly gravitropic [Caspar and Pickard, 1989], but both the pin2 [Müller et al., 1998, Luschnig et al., 1998] and aux1 [Benett et al., 1996, Swarup et al., 2001] null-mutants are agravitropic. Based on this it has been suggested that other, PIN3,7 independent mechanisms for gravitropism exist [Wolverton et al., 2002]. Our study suggests that PIN2 may be a candidate for such a secondary asymmetry generating mechanism, provided that gravitropism can somehow influence PIN2 directly.

Our study is an important step in unraveling the mechanistic basis of halotropism. It can be computed that in the experiments we performed here and earlier [Galvan-Ampudia et al., 2013] the differences in salt concentration at both sides of the root are on the order of 4 to 9.5%. Thus, future studies should be aimed at deciphering how such small asymmetries in auxin levels can become translated into a single sided PIN2 response and how this might be related to the seemingly contradictory findings of an initial increase in PIN2 levels soon after the application of salt stress as observed by Ziewka et al. [Zwiewka et al., 2015] and the reduction in PIN2 levels after 6 hours of salt stress as we reported earlier [Galvan-Ampudia et al., 2013].

In addition, future studies should be aimed at deciphering the interplay between different tropisms. Interestingly, we derived here that the auxin asymmetry generated during halotropism is substantially smaller than that during gravitropism. However, salt has been shown to suppress the gravitropism induced degradation of PIN2 [Galvan-Ampudia et al., 2013] while enhancing the degradation of starch [Sun et al., 2008], explaining why halotropism can at least temporarily overcome gravitropism. In our earlier study we demonstrated

that at low salt concentrations halotropism is insufficiently strong to override gravitropism, while for higher salt concentrations, the eventual takeover of halotropic by gravitropic growth depends on salt concentrations [Galvan-Ampudia et al., 2013], suggesting a quantitative tug of war between the two tropisms. Given the important role of PIN2 and AUX1 in both gravitropism [Chen et al., 1998,Abas et al., 2006,Luschnig et al., 1998,Müller et al., 1998,Benett et al., 1996,Swarup et al., 2001] and halotropism (this study), and the important role of PIN2 in phototropism [Wan et al., 2012], these proteins likely represent the signalling nexus at which different tropism pathways converge and signal integration occurs.

A final important question for future research is how tropisms can function in different developmental or environmental conditions, corresponding to different overall auxin levels. For robust tropic responses to occur, this might imply that tropisms generate and plant cells respond to relative rather than absolute changes in auxin levels, an issue that so far has not been investigated.

Materials and methods

Computational model

Summary of the model

We use a spatially extended, grid-based model of the Arabidopsis root, similar to earlier used models [Grieneisen et al., 2007, Laskowski et al., 2008,Mähönen et al., 2014]. The model incorporates a root tissue architecture with subcellular resolution, cell type and developmental zone specific spatial expression domains and polarity patterns for the auxin exporting PIN proteins and the auxin importing AUX/LAX genes, auxin transport within cells and cell walls and across membranes, and feedback of auxin levels on PIN membrane occupation as well as on AUX/LAX gene expression. The source code for the simulation models can be downloaded from:

from:http://bioinformatics.bio.uu.nl/khwjtuss/HaloRoot/

Baseline Model

Tissue lay-out

We started with a highly simplified, rectangular root model, similar to that used in earlier modeling studies [Grieneisen et al., 2007, Laskowski et al., 2008,Mähönen et al., 2014]. Root tissue was simulated with a spatial resolution of 2 μm on a 80 by 925 μm^2 grid. Individual grid points correspond to either cytoplasm, membrane or cell wall. We assume an average cell width of 8 μm, and simulate a total of 8 columns of cells across the width of our 2D root model, incorporating from outermost to innermost epidermal (blue), cortical (green), endodermal (yellow) and vasculature cells (red). The vasculature is connected to the quiescent center (QC, gray), and the lowest part of the root represents the columella (cyan) (Figure 1A1).

Given that tissue growth occurs on a substantially longer timescale of days relative to the minute to hours timescale on which changes in PIN2, AUX1 and auxin patterns occur in response to salt stress, we ignored tissue growth in the current model. We incorporated a subdivision of the root into a meristematic

(MZ), expansion (EZ) and differentiation zone (DZ) (Figure 1A1) containing cells with a height of 8 μm, 60 μm and 100 μm, respectively. Similar to previous modeling studies we incorporated the PIN polarity patterns typical for each cell type and zone [Grieneisen et al., 2007,Laskowski et al., 2008,Mähönen et al., 2014] (Figure 1A). Together, this results in a reverse fountain auxin flux pattern that generates an auxin maximum in the QC [Grieneisen et al., 2007].

Auxin dynamics

Auxin dynamics were modeled on a grid point level, in a manner similar to earlier studies [Mitchison, 1980, Grieneisen et al., 2007,Mähönen et al., 2014]. For an intracellular grid point *i*,*j* auxin dynamics is described as:

$$\frac{\partial A_{i,j}}{\partial t} = p_A - d_A A_{i,j} + \sum_{i',j'} i_{pas+act} A_{i',j'} - \sum_{i',j'} (e_{pas} + e_{PIN}) A_{i,j} + D_{c,w} \Delta A \qquad (1)$$

In Eqn. 1 p_A is the rate of auxin production per grid point, and d_A the rate of auxin degradation per rate grid point, which are zero for wall points and non-zero cellular grid points (membrane, cytoplasm). $i_{pas+act}$ represents the lumped, active a nd passive import of auxin from all extracellular grid points i', j' that are neighbouring the cellular grid point *i*, *j*, and e_{pas} and e_{PIN} correspond to the passive and active export of auxin from cellular grid point (*i*,*j*) to neighbouring extracellular points (i', j'), respectively. These transport reaction terms only exist for membrane and wall grid points. Auxin fluxes were modeled using linear mass action kinetics. Finally, $D_{c,w}$ represents the diffusion constant for auxin inside the cell (*c*), or inside the wall (*w*) and diffusion occurs only among neighbouring cellular or wall grid points but not between cellular and wall points.

Note that $e_{PIN} = a_{PIN} \times PIN_{mem}$, i.e. rather than being a constant parameter, the rate of PIN mediated active auxin transport depends on membrane PIN levels. Furthermore, $PIN_{mem} = PIN_{pat} \times PIN_{exp}$, that is, PIN membrane levels depend on the product of the PIN prepattern determining maximum relative PIN

level at a particular membrane grid point (PIN_{pat}) and the cellular PIN gene expression level (PIN_{exp})[Mähönen et al., 2014].

To model the connection of the explicitly modeled root section to the not-explicitly modeled rest of the plant we incorporate a shoot derived influx into the vasculature and efflux from the root to the shoot from the non-vasculature tissues, similar to earlier studies [Grieneisen et al., 2007,Mähönen et al., 2014].

Parameter values are listed in Table 1.

Table 1: Model parameter values.

Parameter	Baseline model	Extendend model	units
D_{wall}	40	40	$\mu m^2 s^{-1}$
p_A	0.0005	0.0005	s^{-1}
d_A	0.00005	0.0000725	$[]\, s^{-1}$
D_{cell}	600	600	$\mu m^2 s^{-1}$
AUX/LAX_{exp}	100	100	[]
$i_{pas+act}$	10	10	$\mu m s^{-1}$
i_{pas}	-	2.5	$\mu m s^{-1}$
$a_{AUX/LAX}$	-	0.05	$\mu m s^{-1}$
e_{pas}	1	1	$\mu m s^{-1}$
a_{PIN}	0.2	0.2	$\mu m s^{-1}$
PIN_{pat}: max rel apical PIN	1	1	dimensionless
PIN_{pat}: max rel basal PIN	1	1	dimensionless
PIN_{pat}: max rel lateral PIN	.35	.35	dimensionless
epidermis and cortex cells			
PIN_{pat}: max rel lateral PIN endodermal cells	.1	.1	dimensionless
PIN_{exp}	max 100, auxin dep.	100	[]

$basal_{pinmem}$	-	.1	dimensionless
fb_{pinmem}	-	1.5	dimensionless
sat_{pinmem}	-	10	[]
max_{aux1}	-	0.01	[] s^{-1}
sat_{AUX1}	-	50	[]
d_{AUX1}	-	0.0001	s^{-1}

Extended model

Tissue lay-out

We also developed an extended model incorporating a more realistic, wedge-shaped root tip and root cap tissue (Fig. 1A2). The root tip template was generated by developing an idealised, perfectly symmetric, generalised description based on microscopic root tip pictures. The part of the root tip shootward of the lateral root cap was assumed to be perfectly straight and have constant width. In the part of the root containing the root cap, idealised parabolic functions were used to describe the outer boundary of the root cap, and the boundary between different root cap layers, between lateral root cap and epidermis, epidermis and cortex, cortex and endodermis, endodermis and pericycle, en pericycle and rest of vasculature. In the lower half of this part of the root, a central point was choosen, through which several radial lines were drawn that were used to describe cell-walls in the columella, and lower parts of the lateral root cap, epidermis, ground tissue and vasculature.

Based on experimental data, root cap tissue has a similar PIN polarity pattern as epidermal tissue, but with lower maximum membrane PIN levels [Ditengou et al., 2008]. In the extended model, cell types differ not only in PIN pattern, but also have a cell type specific width of $18\mu m$ for epidermal, $20\mu m$ for cortical, $12\mu m$ for endodermal, $8\mu m$ for the outermost vascular and $6\mu m$ for the remaining vascular cells, in agreement with experimental data and similar to earlier models [Laskowski et al., 2008]. Zone dependent cell height was the same as in the baseline model, except for the curved part of the root tip where columella and lateral root cap cell height increases towards the tip of the root. In the extended model, to create sufficient resolution for the curved cell walls and membranes, a spatial resolution of 1μ was used.

To test the effect of left-right distances between epidermis and lateral root cap on the potential to generate auxin asymmetries we also developed a

variation of the extended model in which these distances were increased (Fig 1A3). Increased distances between the epidermal tissues were generated by increasing the size of the outermost vascular cells to $10\mu m$ and of the remaining vascular cells to $8\mu m$, increasing the distance between left and right epidermis with $16\mu m$. In addition, to also increase the distance between left and right epidermis and root cap in the tip of the root where cell files curve inward the leftmost and rightmost columella cells in each tier were increased in size.

AUX/LAX pre pattern

In the baseline model we assumed a constant, homogeneous distribution of auxin importers, and modeled this using a single lumped permeability value for passive and active auxin import $i_{pas+act}$. However, it is well known that the AUX/LAX proteins involved in active auxin uptake have cell type and root zone specific patterns [Benett et al., 1996, Swarup et al., 2001, Swarup et al., 2005, Péret et al., 2012]. Therefore, we distinguish passive and active auxin import in the extended model. For simplicity, we incorporated a single generalised AUX/LAX protein, which domain of expression is the sum of the experimentally reported expression domains for the distinct AUX/LAX genes (Fig. S2). Similar to active efflux, the rate of active influx is then described by $i_{AUX/LAX} = a_{AUX/LAX} \times AUX/LAX_{mem}$ with $AUX/LAX_{mem} = AUX/LAX_{pat} \times AUX/LAX_{exp}$, where AUX/LAX_{pat} is the predefined spatial presence/absence pattern for where AUX/LAX can be expressed and AUX/LAX_{exp} is the actual cellular gene expression. In addition to this spatially heterogeneous active influx we also incorporate a constant, low level of passive auxin influx, i_{pas}, in all cells. Parameter values are listed in Table 1.

Auxin dependent gene expression of AUX/LAX

In a subset of simulations we incorporate the auxin dependence of AUX/LAX gene expression [Laskowski et al., 2006, Laskowski et al., 2008]. We do this by replacing constant AUX/LAX expression levels (AUX/LAX_{exp}) by

the following cell-level equation for gene expression dynamics:

$$\frac{dAUX/LAX}{dt} = max_{aux/lax} \frac{A^2_{meancell}}{A^2_{meancell} + sat^2_{AUX/LAX}} - d_{AUX/LAX} * AUX/LAX \quad (2)$$

Here $max_{aux/lax}$ is the maximum gene expression rate of AUX/LAX, $sat_{AUX/LAX}$ is the auxin level at which AUX/LAX expression is on its half maximum rate, and $d_{AUX/LAX}$ is the degradation rate of AUX/LAX. Parameter values can be found in Table 1.

Auxin feedback on PIN localization

PIN levels on the membrane not only depend on PIN gene expression levels but also on PIN membrane cycling dynamics. PIN proteins are constantly recycled by internalization from the membrane and subsequent secretion to the membrane [Steinmann and Geldner, 1999, Adamowski and Friml, 2015]. Auxin influences this sub cellular trafficking by limiting the rate of internalization, thus stimulating its own efflux from the cell [Paciorek et al., 2005]. This results in a positive feedback between external auxin and membrane PIN levels.

In a subset of simulations we incorporated this positive feedback on PIN membrane levels. We restricted this positive feedback to the epidermal and root cap tissues that are considered of primary importance for generating the auxin asymmetry underlying root bending. For these cells the PIN membrane equation ($PIN_{mem} = PIN_{pat} * PIN_{exp}$) is replaced by the following grid-level equation:

$$PIN_{mem} = PIN_{pat} * PIN_{exp} * (basal_{pinmem} + fb_{pinmem} * (\frac{A^2_{i,j+1}}{A^2_{i,j+1} + sat^2_{pinmem}})) \quad (3)$$

Here $basal_{pinmem}$ is the minimal fraction of PINs on the membrane in absence of auxin, and fb_{pinmem} is the maximal additional fraction of PINs on the membrane in presence of high levels of auxin. sat_{pinmem} is the auxin level at which this auxin dependent fraction attains its half maximum value. Parameter values can be found in Table 1.

Simulating halotropism

Currently no quantitative data is available showing how changes in PIN2 levels depend on the longitudinal position of a root cell (i.e. distance to the root tip). For simplicity we therefore assume the same constant response to salt along the first 1/3 part of the simulated root tissue, while above this part no response to salt is assumed to occur (Fig. 1A). The salt gradient was assumed to be localised left of the root tip. We considered two different halotropism scenarios. In the first, apical PIN2 levels were decreased by 20% in the epidermis and (if present) root cap at the salt exposed side of the root. In the second scenario, concomittant with a reduction of apical PIN2 levels, a 20% upregulation of lateral PIN2 levels was assumed to occur. Both scenarios were based on the experimental data from Galvan-Ampudia *et al.* [Galvan-Ampudia et al., 2013].

Simulations were run without salt stress until auxin concentrations reached an equilibrium, after which salt-stress was applied.

Analysis methods

Auxin levels may vary both due to the imposed salt gradient as well as due to different model settings. To faithfully compare the extent of auxin asymmetry resulting from a salt gradient under different model settings, we compare auxin levels in the left and right epidermis under salt stress with auxin levels under normal, non-salt stressed conditions with the same model settings. Furthermore, we compute percentage rather than absolute differences relative to these normal auxin levels. Formally this can be written as:

$$\Delta auxin_{salt,l/r} = 100 * \frac{auxin_{salt,l/r} - auxin_{normal}}{auxin_{normal}} \quad (4)$$

Numerical integration & runtime performance

Due to the very fast auxin dynamics, stable integration using simple forward Euler schemes would require very small temporal integration steps ($\Delta t = 0.0001\text{s}$) making simulations prohibitively slow. Therefore, a semi-implicit

alternating direction integration scheme [Peaceman and Rachford, 1955] was used that allows for integration timesteps of $\Delta t = 0.2s$. This approach has been extensively validated in earlier studies [Grieneisen et al., 2007,Mähönen et al., 2014].

All simulations were run on a dell Precision T7500 workstation with Intel® Xeon X5680 processor. The code for the model was written in C++. Run time for simulations were typically around 24 hours (corresponding to a biological time of a few days) to reach steady state gene expression and auxin levels in absence of salt stress, and 3-6 hours for simulating salt stress (biological time of 10-36 hours).

Experiments

Growth conditions and treatments

We used *Arabidopsis thaliana* PIN1-GFP [Benková et al., 2003], PIN3-GFP [of PIN-mediated auxin efflux in apical hook development of Arabidopsis thaliana., 2010], pin1 (SALK_047613) and AUX1-mVenus [Band et al., 2014] lines, all in Col-0 background. Seeds were sterilized using a 50% bleach solution. After 2 days of stratification the seeds were germinated on 0.5 MS plates, with 0,1% MES bffer, 1% sucrose, 1% Daishin agar after which the pH was adjusted to 5.8 (using KOH). The plates were placed at an angle of 70 degrees and placed in a climate chamber ($22^{\circ}C$ at long day conditions, 16 hours of light at 130 umol/m2/s). After 4 days the plants were transferred to new 0.5 MS plates. On day 5 the treatment was started. Salt gradients were created starting at 0.5 cm from the root tip by cutting the left lower corner of the square 0.5 MS plate and replacing this with fresh 0.5 MS medium containing 125mM, 200mM or 300 mM NaCl, depending on the experiment (for control plates medium was replaced with fresh 0.5 MS medium without salt). The plates were dried for 15 minutes and placed back into the climate chamber. Microscopy slides were prepared by cutting a rectangle around the seedling and placing it upside down on a microscopy slide while kept at an angle of 70 degrees. The

slides were imaged within 5 minutes after removing the plates from the climate chamber.

Confocal laser scanning microscopy

The images were acquired using a Nikon Ti inverted microscope in combination with an A1 spectral confocal scanning head. For the GFP the excitation wavelength used was 488, the emission wavelength that was detected was 505-555. For mVenus (YFP) the excitation wavelength used was 514nm and the emission wavelength used was 525-555. The analysis of the images was performed using FIJI (Fiji Is Just Image-J, http://_ji.sc/Fiji) software.

Analysis

PIN1 and PIN3 response to salt gradient

Plants were exposed to a 300mM NaCl gradient and imaged at different time points (0.5, 1, 2, 3 and 6 hours). For control plants no significant differences between time points were found. Therefore, all control plants could be pooled into a single control group. Three biological replicates were performed for both PIN1 and PIN3, each time with newly grown A. thaliana seedlings. In each experiment 6 roots were imaged for the control condition, 2 roots for the 0.5 hours of salt gradient and 4 roots for the other treatments (1hour, 2 hours, 3 hours and 6 hours). Five cells from each root were used for the quantification of PIN membrane levels. We dismissed images in which an insufficient number of cells could be used for quantifying PIN membrane levels. This could be due to an unfortunate root angle, bad confocal plane or air bubbles near the root while imaging. Five cells of each imaged root were used to determine the average GFP intensity of the pixels by drawing a Region of Interest (ROI) around one side of the membrane or the intracellular part of the cell and using FIJI software to calculate the average. These values were then corrected for background fluorescence by subtracting the average value of a part of the root which does not express the specific PIN protein. Significance levels between control and salt conditions and the different time points were tested by

using ANOVA (using SPSS software).

AUX1 response to salt gradient

Plants were imaged 3 hours after exposure to a 300mM salt gradient or control conditions. Three biological replicates were performed for the salt gradient and for control conditions. For the salt gradient a total of 13 plants were analysed (5, 4 and 4 for the individual replicates), for control conditions a total of 9 plants were analysed (4, 3 and 2 for the individual replicates). For each root a line transversal to the longitudinal axis of the root was drawn to indicate the position at which the lateral root cap ends. Next, two lines were drawn following the outer lateral membranes of the epidermal cells starting from the end of the rootcap in the shootward direction (see Fig 3C, right). YFP intensity levels of the pixels composing these lines were determined using ImageJ software (http://rsbweb.nih.gov/ij). For each root, we computed the ratios between left and right epidermal AUX1 levels as a function of distance from the lateral root cap by determining the ratio of YFP intensity levels for pixel pairs consisting of a pixel at the left and a pixel at the right outer epidermal membrane located at the same distance from the end of the lateral root cap. For the salt treatment 1 root was discarded from our analysis, for the control conditions 2 roots were discarded from our analysis because of bad confocal planes resulting in highly uneven fluorescence levels at the left and right sides of the root prohibiting the proper application of the above explained analysis method. In addition, for control conditions 1 root was discarded from our analysis because of the high level of root bending observed. It has been previously shown that root bending may induce local elevation of AUX1 levels [26]. Ratios computed for salt gradient and control roots were binned per 5000 micron length segments. Significance levels between control and salt gradient exposed roots were computed per bin using a double sided T-test (using R software).

pin1 effect on halotropism

Seeds from a heterozygous pin1 mutants (SALK_047613) (the homozygous pin1 mutant is sterile [Okada et al., 1991]) were plated and grown to an age of 5 days as described above (growth conditions and treatment). A difference relative to the above described experiments is that the plants were not transferred after 4 days to new 0.5 MS plates but were germinated on the final treatment plates. On day 5 the treatment was started, as described above. The 5-day old seedlings were then analysed for their halotropic response according to Galvan-Ampudia et al. [Galvan-Ampudia et al., 2013]. Ten seeds were used per plate and 20 plates for each treatment (0, 125 and 200 mM of NaCl). All seedlings were genotyped to identify seedlings homozygous for the tDNA insertion (forward genomic primer: acggtatagtccctctataact, reverse genomic primer: gctgcaaaagagtgacataaa and insertion primer (LBb1.3): attttgccgatttcggaac). Significance levels between genotypes at different time points were tested with SPSS software by using MANOVA (post-hoc Bonferroni $p<0.01$).

Acknowledgements

We would like to thank Paulien Hogeweg for helpfull discussions. We would like to thank Laurens Krah and Daniel Weisse for their advice on the AUX1 analysis. We thank Teva Vernoux (PIN1-GFP), Eva Benkova (PIN3-GFP), Remko Offringa (pin1) and Malcolm Bennett (AUX1-mVenus) for published and unpublished materials. We would also like to thank Remko Offringa and Chris van Schie for advice on the pin1 experiment.

Competing interests

No competing interests declared

Author contributions

TvdB constructed the code for halotropism simulations, conceived and conducted the computer simulations, and wrote the manuscript. RAK conceived and conducted the halotropism experiments. CT conceived the halotropism experiments and wrote the manuscript. KtT constructed the main simulation code, conceived the halotropism simulations, and wrote the manuscript.

Funding

TvdB and KtT are supported by VIDI grant 864.14.003 of the Netherlands Scientific Organization (NWO). RAK and CT are supported by chemical sciences grant 711.014.002 of the Netherlands Scientific Organization (NWO)

References

[Abas et al., 2006] Abas, L., Benjamins, R., Malenica, N., Paciorek, T., Wisniewka, J., Moulinier-Anzola, J., Sieberer, T., Friml, J., and Luschnig, C. (2006). Intracellular trafficking and proteolysis of the arabidopsis auxin-efflux facilitator pin2 are involved in root gravitropism. *Nature Cell Biology*, 8:249–256.

[Adamowski and Friml, 2015] Adamowski, M. and Friml, J. (2015). Pin-dependent auxin transport: Action, regulation, and evolution. *The Plant Cell*, 27(1):20–32.

[Aquea et al., 2012] Aquea, F., Federici, F., Moscoso, C., Vega, A., Jullian, P., Haselhoff, J., and Arce-Johnson, P. (2012). A molecular framework for the inhibition of arabidopsis root growth in response to boron toxicity. *Plant, Cell & Environment*, 35(4):719–734.

[Band et al., 2014] Band, L. R., Wells, D. M., Fozard, J. A., Ghetiu, T., French, A. P., Pound, M. P., Wilson, M. H., Yu, L., Li, W., Hijazi, H. I., Oh, J., Pearce, S. P., Perez-Amador, M. A., Yun, J., Kramer, E., Alonso, J. M., Godin, C., Vernoux, T., Hodgman, T. C., Pridmore, T. P., Swarup, R., King, J. R., and Bennett, M. J. (2014). Systems analysis of auxin transport in the arabidopsis root apex. *The Plant Cell*, 26(3):862–875.

[Band et al., 2012] Band, L. R., Wells, D. M., Larrieu, A., Sun, J., Middleton, A. M., French, A., Brunoud, G., Sato, E. M., Wilson, M. H., Péret, B., Oliva, M., Swarup, R., Sairanen, I., Parry, G., Ljung, K., Beeckman, T., Garibaldi, J. M., Estelle, M., Owen, M. R., Vissenberg, K., Hodgman, T. C., Pridmore, T. P., King, J. R., Vernoux, T., and Bennett, M. J. (2012). Root gravitropism is regulated by a transient lateral auxin gradient controlled by a tipping-point mechanism. *Proceedings of the National Academy of Sciences*, 109(12):4668–4673.

[Baster et al., 2012] Baster, P., Robert, S., Kleine-Vehn, J., Vanneste, S., Kania, U., Grunewald, W., De Rybel, B., Beeckman, T., and Friml, J. (2012). Scftir1/afb-auxin signalling regulates pin vacuolar trafficking and auxin fluxes during root gravitropism. *The EMBO Journal*, 32(2):260–274.

[Benett et al., 1996] Benett, M., Marchant, A., Green, H., May, S., Ward, S., Millner, P., Walker, A., Schulz, B., and Feldmann, K. (1996). Arabidopsis aux1 gene: a permease-like regulator of root gravitropism. *Science*, 273:948–950.

[Benková et al., 2003] Benková, E., Michniewicz, M., Sauer, M., Teichmann, T., Seifertová, D., Jürgens, G., and Friml, J. (2003). Local, efflux-dependent auxin gradients as a common module for plant organ formation. *Cell*, 115(5):591 – 602.

[Blilou et al., 2005] Blilou, I., Xu1, J., Wildwater, M., Willemsen, V., Paponov, I., Friml, J., Heidstra, R., Aida, M., Palme, K., and Scheres, B. (2005). The pin auxin efflux facilitator network controls growth and patterning in arabidopsis roots. *Nature*, 433:39–44.

[Brunoud et al., 2012] Brunoud, G., Wells, D., Oliva, M., Larrieu, A., Mirabet, V., Burrow, A., Beeckman, T., Kepinski, S., Traas, J., Bennett, M., and Vernoux, T. (2012). A novel sensor to map auxin response and distribution at high spatio-temporal resolution. *Nature*, 482(7383):103–106.

[Caspar and Pickard, 1989] Caspar, T. and Pickard, B. (1989). Gravitropism in a starchless mutant of arabidopsis: implications for the starch-statolith theory of gravity sensing. *Planta*, 177:185–197.

[Chapman et al., 2011] Chapman, N., Whalley, W. R., Lindsey, K., and Miller, A. J. (2011). Water supply and not nitrate concentration determines primary root growth in arabidopsis. *Plant, Cell & Environment*, 34(10):1630–1638.

[Chen et al., 1998] Chen, R., Hilson, P., Sedbrook, J., Rosen, E., Caspar, T., and Masson, P. H. (1998). The arabidopsis thaliana agravitropic 1 gene encodes a component of the polar-auxin-transport efflux carrier. *Proceedings of the National Academy of Sciences*, 95(25):15112–15117.

[Cruz-Ramírez et al., 2012] Cruz-Ramí-rez, A., Díaz-Triviño, S., Blilou, I., Grieneisen, V., Sozzani, R., Zamioudis, C., Miskolczi, P., Nieuwland, J., Benjamins, R., Dhonukshe, P., Caballero-Pérez, J., Horvath, B., Long, Y., Mähönen, A., Zhang, H., Xu, J., Murray, J., Benfey, P., Bako, L., Marée, A., and B., S. (2012). A bistable circuit involving scarecrow-retinoblastoma integrates cues to inform asymmetric stem cell division. *Cell*, 150:1002–1015.

[Ditengou et al., 2008] Ditengou, F. A., Teale, W. D., Kochersperger, P., Flittner, K. A., Kneuper, I., van der Graaff, E., Nziengui, H., Pinosa, F., Li, X., Nitschke, R., Laux, T., and Palme, K. (2008). Mechanical induction of lateral root initiation in arabidopsis thaliana. *Proceedings of the National Academy of Sciences*, 105(48):18818–18823.

[Eshel and Beeckman, 2013] Eshel, A. and Beeckman, T., editors (2013). *Plant Roots: The Hidden Half, Fourth Edition*. CRC press.

[Friml et al., 2002a] Friml, J. ., Wisniewka, J., Benkova, E., Mendgen, K., and Palme, K. (2002a). Lateral relocation of auxin efflux regulator pin3 mediates tropism in arabidopsis. *Nature*, 415:806–809.

[Friml et al., 2002b] Friml, J., Benkova, E., Blilou, I., Wisniewska, J., Hamann, T., Ljung, K., Woody, S., Sandberg, G., Scheres, B., Jurgens, B., and Palme, K. (2002b). Atpin4 mediates sink-driven auxin gradients and root patterning in arabidopsis. *Cell*, 108:661–673.

[Friml et al., 2003] Friml, J., Vieten, A., Sauer, M., Weijers, D., Schwarz, H., Hamann, T., Offringa, R., and Jurgens, G. (2003). Efflux-dependent auxin gradients establish the apical-basal axis of arabidopsis. *Nature*, 426:147–153.

[Galvan-Ampudia et al., 2013] Galvan-Ampudia, G., Julkowska, M., Darwish, E., Gandullo, J., and Korver, R. (2013). Halotropism is a response of plant roots to avoid a saline environment. *Current Biology*, 23:2044–2050.

[Grieneisen et al., 2007] Grieneisen, V., Xu, J., Maree, A., Hogeweg, P., and Scheres, B. (2007). Auxin transport is sufficient to generate a maximum and gradient guiding root growth. *Nature*, 449:1008–1013.

[Jain et al., 2007] Jain, A., Poling, M. D., Karthikeyan, A. S., Blakeslee, J. J., Peer, W. A., Titapiwatanakun, B., Murphy, A. S., and Raghothama, K. G. (2007). Differential effects of sucrose and auxin on localized phosphate deficiency-induced modulation of different traits of root system architecture in arabidopsis. *Plant Physiology*, 144(1):232–247.

[Kleine-Vehn et al., 2010] Kleine-Vehn, J., Ding, Z., Jones, A., Tasaka, M., Morita, M., and friml, J. (2010). Gravity-induced pin transcytosis for polarization of auxin fluxes gravity-sensing root cells. *PNAS*, 107:22344–22349.

[Kleine-Vehn et al., 2008] Kleine-Vehn, J., Leitner, J., Zwiewka, M., Sauer, M., Abas, L., Luschnig, C., and Friml, J. (2008). Differential degradation of pin2 auxin efflux carrier by retromer-dependent vacuolar targeting. *Proceedings of the National Academy of Sciences of the United States of America*, 105(46):17812–17817.

[Laskowski et al., 2006] Laskowski, M., Biller, S., Stanley, K., Kajstura, T., and Prusty, R. (2006). Expression profiling of auxin-treated arabidopsis roots: Toward a molecular analysis of lateral root emergence. *Plant Cell Physiology*, 47:788–792.

[Laskowski et al., 2008] Laskowski, M., Grieneisen, V., Hofhuis, H., ten Hove, C., Hogeweg, P., Maree, A., and Scheres, B. (2008). Root system architecture from coupling cell shape to auxin transport. *Plos Biology*, 6:e307.

[Laxmi et al., 2008] Laxmi, A., Pan, J., Morsy, M., and Chen, R. (2008). Light plays an essential role in intracellular distribution of auxin. *PLoS ONE*, 3(1):e1510.

[Liu et al., 2015] Liu, W., Li, R.-J., Han, T.-T., Cai, W., Fu, Z.-W., and Lu, Y.-T. (2015). Salt stress reduces root meristem size by nitric oxide-mediated modulation of auxin accumulation and signaling in arabidopsis. *Plant Physiology*, 168(1):343–356.

[Ljung et al., 2005] Ljung, K., Hull, A. K., Celenza, J., Yamada, M., Estelle, M., Normanly, J., and Sandberg, G. (2005). Sites and regulation of auxin biosynthesis in arabidopsis roots. *The Plant Cell*, 17(4):1090–1104.

[Luschnig et al., 1998] Luschnig, C., Gaxiola, R., Grisafi, P., and Fink, G. (1998). Eir1, a root-specific protein involved in auxin transport, is required for gravitropism in arabidopsis thaliana. *Genes & Development*, 12:2175–2187.

[Mironova et al., 2010] Mironova, V., Omelyanchuk, N., Yosiphon, G., Fadeev, S., Kolchanov, N., Mjolsness, E., and Likhoshvai, V. (2010). A plausible mechanism for auxin patterning along the developing root. *BMC systems biology*, 4.

[Mitchison, 1980] Mitchison, G. (1980). A model for vein formation in higher plants. *Proceedings of the Royal Society of London - Biological Sciences*, 207:79–109.

[Mullen et al., 1998] Mullen, J., Ishiwaka, H., and Evans, M. (1998). Analysis of changes in relative elemental growth rate patterns in the elongation zone of arabidopsis roots upon gravistimulation. *Plant*, 206:598–603.

[Mähönen et al., 2014] Mähönen, A., Ten Tusscher, K., Siligato, R., Smetana, O., and Diaz-Trivino, S. (2014). Plethora gradient formation mechanism separates auxin responses. *Nature*, 0:1–5.

[Müller et al., 1998] Müller, A., Guan, C., Gälweiler, L., Tänzler, P., Huijser, P., Marchant, A., Parry, G., Bennett, M., Wisman, E., and Palme, K. (1998). Atpin2 defines a locus of arabidopsis for root gravitropism control. *The EMBO Journal*, 17(23):6903–6911.

[Niu et al., 2015] Niu, Y., Jin, G., Li, X., Tang, C., Zhang, Y., Liang, Y., and Yu, J. (2015). Phosphorus and magnesium interactively modulate the elongation and directional growth of primary roots in arabidopsis thaliana (l.) heynh. *Journal of Experimental Botany*, 66(13):3841–3854.

[of PIN-mediated auxin efflux in apical hook development of Arabidopsis thaliana., 2010] of PIN-mediated auxin efflux in apical hook development of Arabidopsis thaliana., R. (2010). Zádníková, p and petrásek, j and marhavy, p and raz, v and vandenbussche, f and ding, z and schwarzerová, k and morita, mt and tasaka, m and hejátko, j and van der straeten, d and friml, j and benková, e. *Development*, 137:607–617.

[Okada et al., 1991] Okada, K., Ueda, J., Komaki, M. K., Bell, C. J., and Shimura, Y. (1991). Requirement of the auxin polar transport system in early stages of arabidopsis floral bud formation. *The Plant Cell*, 3(7):677–684.

[Paciorek et al., 2005] Paciorek, T., Zazimalova, E., Ruthardt, N., Petrasek, J., and Stierhof, Y. (2005). Auxin inhibits endocytosis and promotes its own efflux from the cells. *Nature*, 435:1251–1256.

[Paponov et al., 2005] Paponov, I. A., Teale, W. D., Trebar, M., Blilou, I., and Palme, K. (2005). The {PIN} auxin efflux facilitators: evolutionary and functional perspectives. *Trends in Plant Science*, 10(4):170 – 177.

[Peaceman and Rachford, 1955] Peaceman, D. W. and Rachford, H. H. (1955). The numerical solution of parabolic and elliptic differential equations. *Journal of the Society for Industrial and Applied Mathematics*, 3:28–41.

[Petrasek et al., 2006] Petrasek, J., Mravec, J., Bouchard, R., Blakeslee, J., Abas, M., Seifertova, D., Wisniewska, J., Tadele, Z., Kubes, M., Covanova, M., Dhonukshe, P., Skupa, P., Benkova, E., Perry, L., Krecek, P., Lee, O., Fink, G., Geisler, M., Murphy, A., Luschnig, C., Zazimalova, E., and Friml, J. (2006). Pin proteins perform a rate-limiting function in cellular auxin efflux. *Science*, 312:914–918.

[Péret et al., 2012] Péret, B., Swarup, K., Ferguson, A., Seth, M., Yang, Y., Dhondt, S., James, N., Casimiro, I., Perry, P., Syed, A., Yang, H., Reemmer, J., Venison, E., Howells, C., Perez-Amador, M. A., Yun, J., Alonso, J., Beemster, G. T., Laplaze, L., Murphy, A., Bennett, M. J., Nielsen, E., and Swarup, R. (2012). Aux/lax genes encode a family of auxin influx transporters that perform distinct functions during arabidopsis development. *The Plant Cell*, 24(7):2874–2885.

[Rakusová et al., 2011] Rakusová, H., Gallego-Bartolomé, J., Vanstraelen, M., Robert, H. S., Alabadí, D., Blázquez, M. A., Benková, E., and Friml, J. (2011). Polarization of pin3-dependent auxin transport for hypocotyl gravitropic response in arabidopsis thaliana. *The Plant Journal*, 67(5):817–826.

[Rutschow et al., 2014] Rutschow, H., Baskin, T., and Kramer, E. (2014). The carrier auxin resistant (aux1) dominates auxin flux into arabidopsis protoplasts. *New Phytologist*, 204:536–544.

[Sassi et al., 2012] Sassi, M., Lu, Y., Zhang, Y., Wang, J., Dhonukshe, P., Blilou, I., Dai, M., Li, J., Gong, X., Jaillais, Y., Yu, X., Traas, J., Ruberti, I., Wang, H., Scheres, B., Vernoux, T., and Xu, J. (2012). Cop1 mediates the coordination of root and shoot growth by light through modulation of pin1- and pin2-dependent auxin transport in arabidopsis. *Development*, 139(18):3402–3412.

[Scheitz et al., 2013] Scheitz, K., Lüthen, H., and Schenck, D. (2013). Rapid auxin-induced root growth inhibition requires the tir and afb auxin receptors. *Planta*, 238(6):1171–1176.

[Steinmann and Geldner, 1999] Steinmann, T. and Geldner, N. (1999). Coordinated polar localization of auxin efflux carrier pin1 by gnom arf gef. *Science*, 286(5438):316.

[Stepanova et al., 2008] Stepanova, A., Robertson-Hoy, J., Yun, J., Benavente, L., Xie, D., Dolezal, K., Schlereth, A., Jürgens, G., and J.M., A. (2008). Taa1-mediated auxin biosynthesis is essential for hormone crosstalk and plant development. *Cell*, 133:177–191.

[Sukumar et al., 2009] Sukumar, P., Edwards, K. S., Rahman, A., DeLong, A., and Muday, G. K. (2009). Pinoid kinase regulates root gravitropism through modulation of pin2-dependent basipetal auxin transport in arabidopsis. *Plant Physiology*, 150(2):722–735.

[Sun et al., 2008] Sun, F., Zhang, W., Hu, H., Li, B., Wang, Y., Zhao, Y. ad Li, K., Liu, M., and Li, X. (2008). Salt modulates gravity signaling pathway to regulate growth direction of primary roots in arabidopsis. *Plant Physiology*, 146:178–188.

[Swarup et al., 2008] Swarup, K., Benkova, E., Swarup, R., Casimiro, I., Peret, B., Yang, Y., Parry, G., Nielsen, E., De Smet, I., Vanneste, S., Levesque, M., Carrier, D., , James, n., Calvo, V., Ljung, K., Kramer, E., Roberts, R., Graham, N., Marillonnet, S., and Patel, K. e. a. (2008). The auxin influx carrier lax3 promotes lateral root emergence. *Nature Cell Biology*, 10:946–954.

[Swarup et al., 2001] Swarup, R., Friml, J., Marchant, A., Ljung, K., Sandberg, G., Palme, K., and Bennett, M. (2001). Localization of the auxin permease aux1 suggests two functionally distinct hormone pathways operate in the arabidopsis root apex. *Genes Development*, 15:2648–2653.

[Swarup et al., 2005] Swarup, R., Kramer, E., Perry, P., Knox, K., Leyser, H., Haseloff, J., Beemster, G., Bhalerao, R., and Bennett, M. (2005). Root gravitropism requires lateral root cap and epidermal cells for transport and response to a mobile auxin signal. *Nature Cell Biology*, pages 1057 – 1065.

[Thimann, 1936] Thimann, K. (1936). Auxins and the growth of roots. *American Journal of Botany*, 23(8):561–569.

[Tian et al., 2014] Tian, H., De Smet, I., and Z., D. (2014). Shaping a root system: regulating lateral versus primary root growth. *Trends in Plant Science*, 19:426–341.

[Wan et al., 2012] Wan, Y., Jasik, J., Wang, L., Hao, H., Volkmann, D., Menzel, D., Mancuso, S., Baluska, F., and Lina, J. (2012). The signal transducer nph3 integrates the phototropin1 photosensor with pin2-based polar auxin transport in arabidopsis root phototropism. *The Plant Cell*, 24:551â€“565.

[Went, 1974] Went, F. W. (1974). Reflections and speculations. *Annual Review of Plant Physiology*, 25(1):1–27.

[West et al., 2004] West, G., Inzé, D., and Beemster, G. (2004). Cell cycle modulation in the response of the primary root of arabidopsis to salt stress. *Plant Physiology*, 135(2):1050–1058.

[Whitford et al., 2012] Whitford, R., Fernandez, A., Tejos, R., Pérez, A., Kleine-Vehn, J., Vanneste, S., Drozdzecki, A., Leitner, J., Abas, L., Aerts, M., Hoogewijs, K., Baster, P., De Groodt, R., Lin, Y., Storme, V., Van de Peer, Y., Beeckman, T., Madder, A., Devreese, B., Luschnig, C., Friml, J., and Hilson, P. (2012). Golven secretory peptides regulate auxin carrier turnover during plant gravitropic responses. *Developmental Cell*, 22:678–685.

[Wisniewska et al., 2006] Wisniewska, J., Xu, J., Seifertová, D., Brewer, P., Ruzicka, K., Blilou, I., Rouquie, D., Benkova, E., Scheres, B., and Friml, J. (2006). Polar pin localization directs auxin flow in plants. *Science*, 312:883.

[Wolverton et al., 2002] Wolverton, C., Mullen, J., Ishikawa, H., and ML., E. (2002). Root gravitropism in response to a signal originating outside of the cap. *Planta*, 215:153–157.

[Zhu et al., 1998] Zhu, T., Lucas, W. J., and Rost, T. L. (1998). Directional cell-to-cell communication in thearabidopsis root apical meristem i. an ultrastructural and functional analysis. *Protoplasma*, 203:35–47.

[Zwiewka et al., 2015] Zwiewka, M., Nodzyński, T., Robert, S., Vanneste, S., and Friml, J. (2015). Osmotic stress modulates the balance between exocytosis and clathrin-mediated endocytosis in arabidopsis thaliana. *Molecular Plant*, 8:1175–1187.

Figures

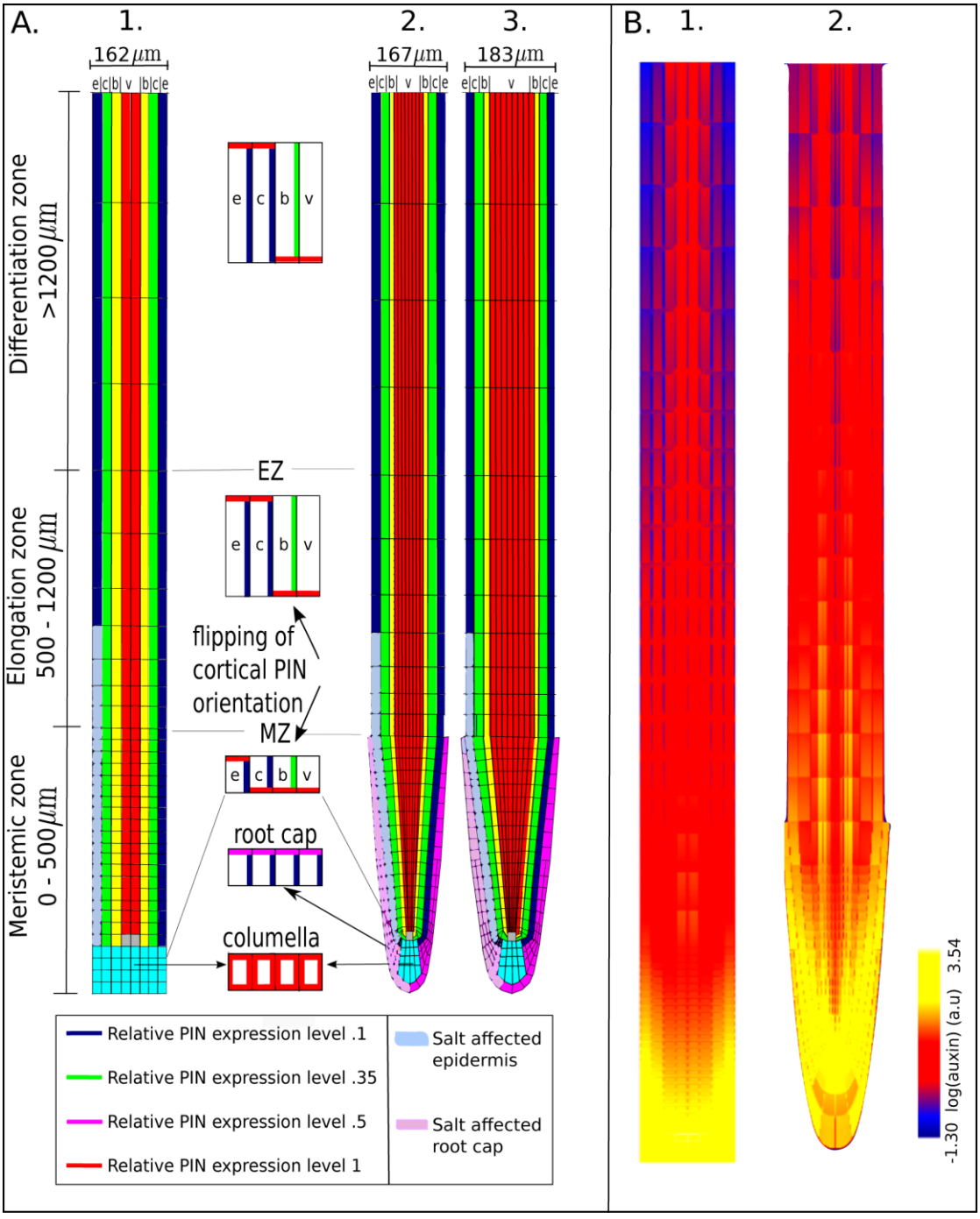

Figure 1. Overview of model tissue layout.

A Layout of cell types, root zones and PIN polarity pattern in the baseline (**1**) and extended (**2**) root model and a variant of the extended root model with

larger left-right distances (**3**). Quiescent center (grey), Columella (cyan), Root Cap (pink), Epidermis (e, blue), Cortex (c, green), Border or endodermal cells (b, yellow) and Vasculature (v, red). The root is divided into 3 zones, from bottom to top: meristem (MZ), elongation (EZ) and differentiation zone (DZ). Insets in the middle shows the predefined PIN polarity pattern as present on the left side of the root in the different root zones (right side is a mirror image of the left side). An imposed salt gradient is assumed to influence PIN2 levels in lower left epidermal cells (light blue) and root cap cells (light pink).

B Steady state non-salt stressed auxin pattern in the baseline (**1**) and extended model (**2**).

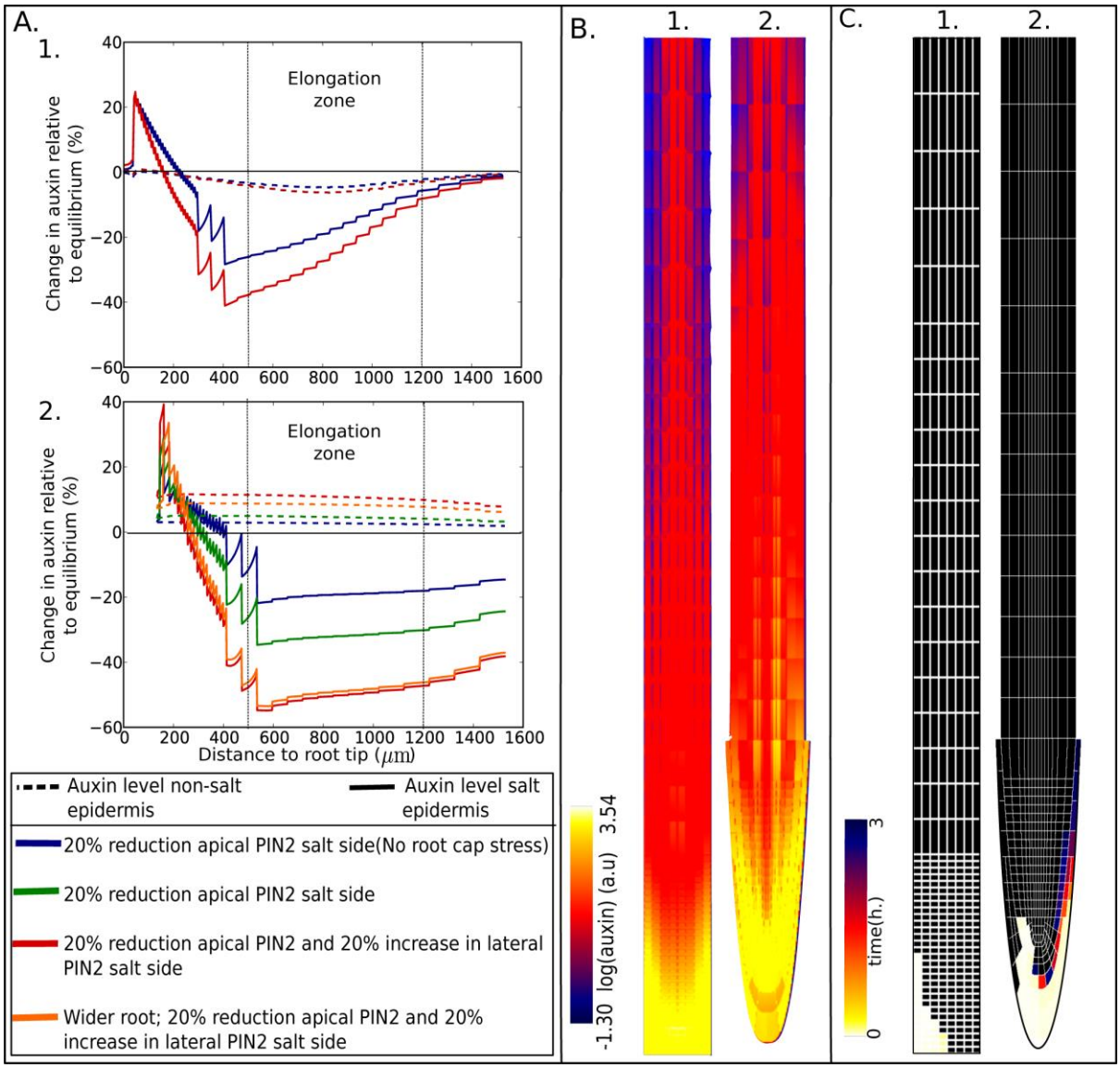

Figure 2. Influence of salt-induced PIN2 changes.

Salt-stress was applied to the baseline (**1**) and extended model (**2**), either through only reducing apical PIN2 levels, or additionally also increasing lateral PIN2 levels. To investigte the impact of having a root cap, in the extended model the reduction in apical PIN2 levels was applied only in epidermal cells, or in epidermal and root cap cells. To investigate the impact of distances between epidermal and root cap cells, results are also shown for an alternative realistic root tip architecture with increased left-right distances between

epidermal and root cap cells, applying salt stress by decreasing apical and increasing lateral PIN2 levels. (**A**) Percentage changes in epidermal auxin levels on the salt-stressed and non-stressed side of the root relative to non-stressed conditions. Location of the elongation zone is indicated.

(**B**) Overall root tip auxin distributions for the scenario resulting in most auxin asymmetry in the baseline (**1**) and extended (**2**) model after 24 hours of salt-stress.

(**C**) Auxin rerouting maps for the scenario resulting in most auxin asymmetry in the baseline (**1**) and extended (**2**) model. For the baseline model, auxin rerouting was monitored by measuring the time at which at least a 1% increase in auxin levels occured. For the extended model, a 10% auxin increase threshold was applied.

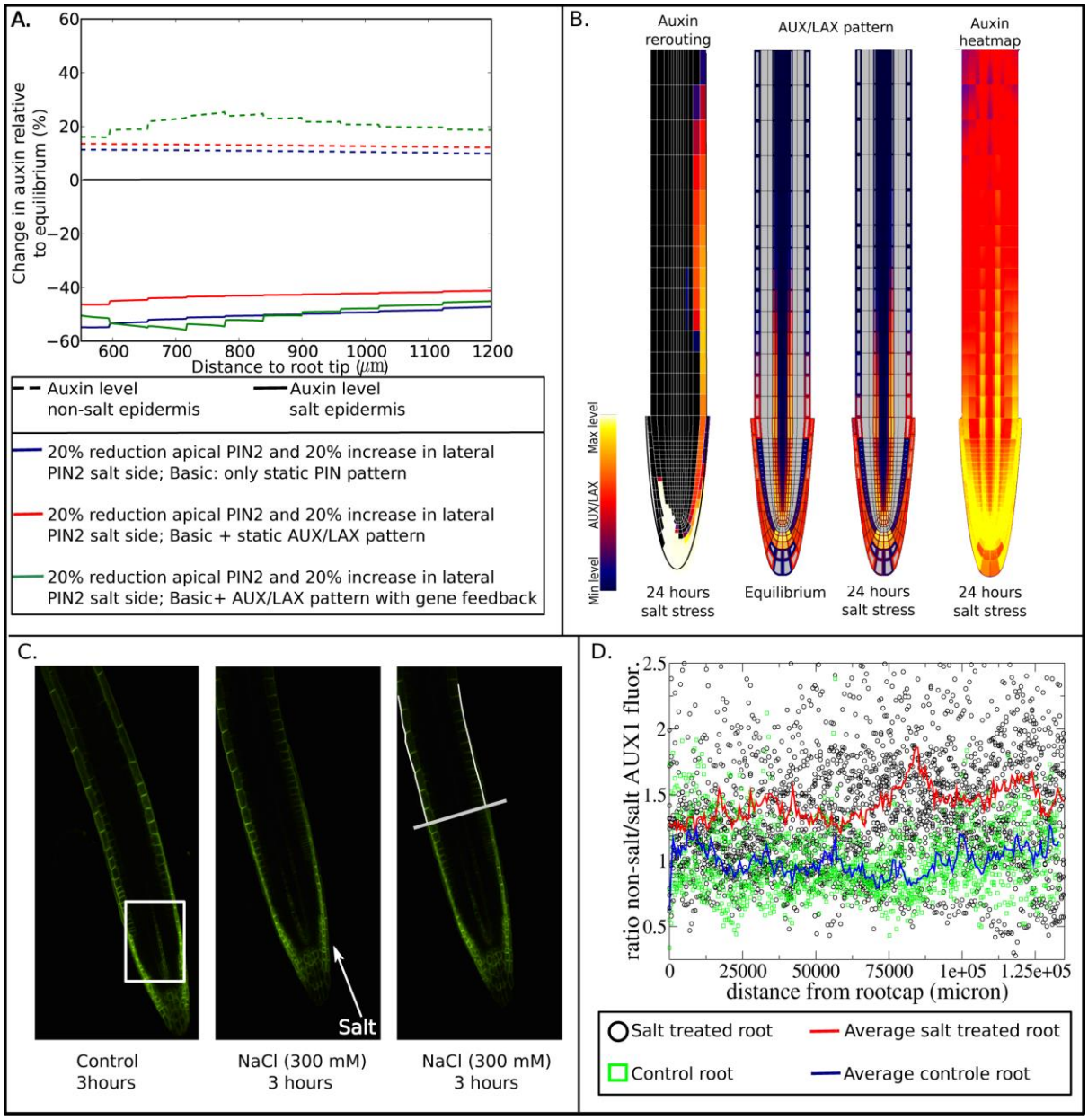

Figure 3. Role of auxin dependent AUX/LAX

A Impact of AUX/LAX pattern and auxin feedback on AUX/LAX expression on epidermal auxin assymetry after 24 hours of applying salt stress by reducing apical and increasing lateral PIN2 levels.

B Auxin rerouting, change in AUX/LAX expression pattern and resulting auxin asymmetry in presence of auxin feedback on AUX/LAX expression.

C AUX1-mVenus pattern in control root showing in the boxed region an asymmetric AUX1 fluorescence in the vasculature due to root orientation (left), and in a salt-exposed root showing generation of an asymmetric AUX1 pattern in the epidermis (middle). The right picture shows a line transversal to the root length axis indicating the end of the lateral root cap, and two lines tracking the outer epidermal membrances in which AUX1 fluorescence levels are measured from the end of the root cap shootward.

D Ratios in AUX1 fluorescence levels of the non-salt exposed to the salt-exposed side as a function of distance from the lateral root cap. For control, data from 6 roots were used, for salt treated conditions data from 12 roots were used. For details see Methods

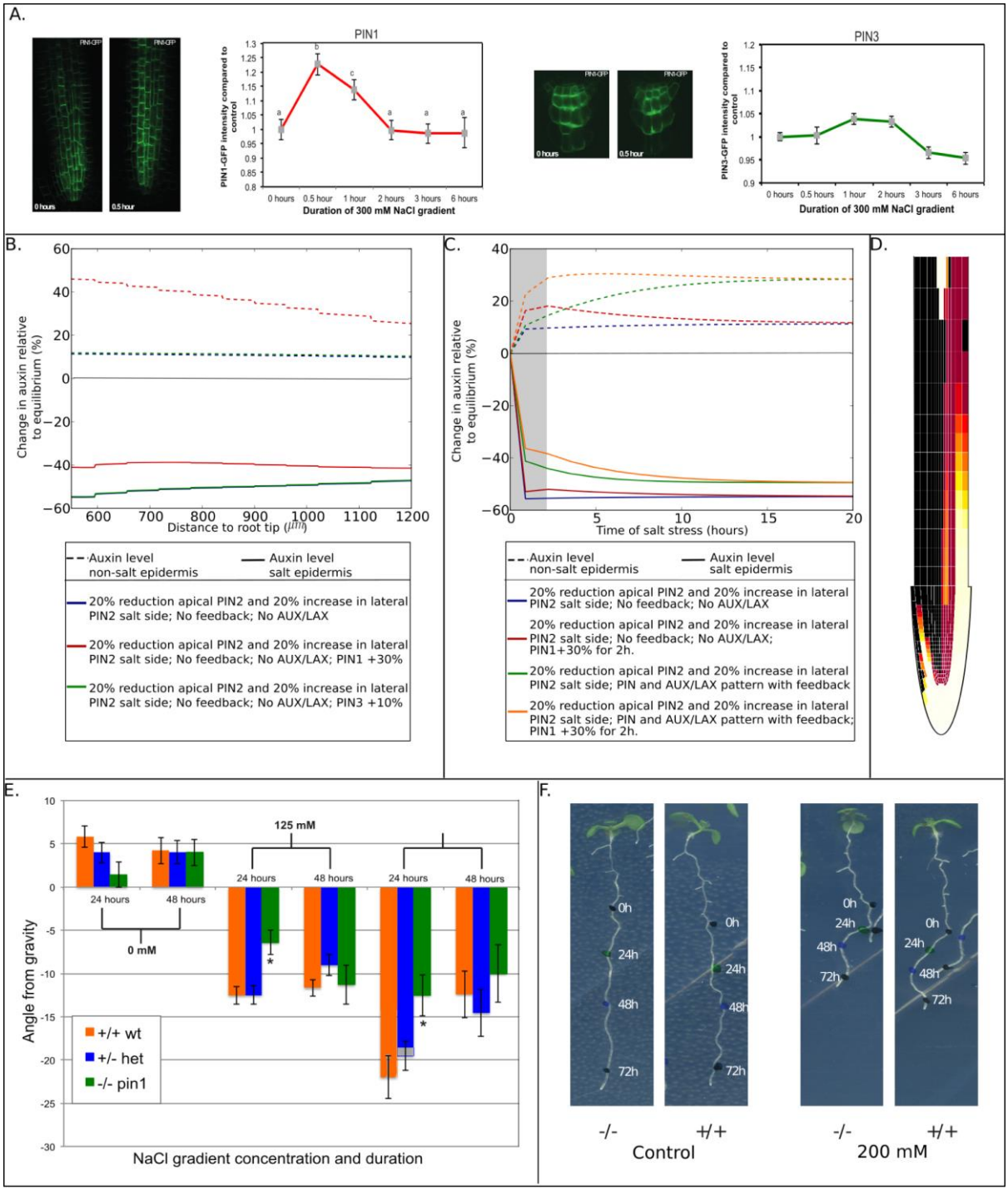

Figure 4. Influence of salt gradient induced changes in PIN1 and PIN3.

Representative pictures of roots of A. thaliana seedlings expressing PIN1-

GFP (**A, first and second**) or PIN3-GFP (**A, fourth and fifth**) in control conditions (**A, first and fourth**) and after 30 minutes of a 300 mM NaCl gradient (**A, second and fifth**). (**A third and sixt**) Quantification of total PIN1-GFP (**A, third**) or total PIN3-GFP (**A, sixth**) intensity in A. thaliana stele root cells at different time points. Three independent biological replicates were used in which 2 to 6 roots were used per time point and 5 stele cells were analysed per root. For PIN1 n=90 for 0 hours, n=25 for 0.5 hour, n=55 for 1 hour and 2 hours, n=50 for 3 hours and 6 hours, for PIN3 n=70 for 0 hours, n=20 for 0.5 hour, n=60 for 1 hour, n=55 for 2 hours, n=40 for 3 hours and n=35 for 6 hours. Letters show different significance groups as determined by multivariate ANOVA. PIN1 levels show a 22% increase relative to control after 30 minutes of exposure to a salt gradient, a fter 1 hour this increase is reduced to 14%, and after 2 hours the PIN1 level showed no significant difference relative to the control condition. PIN3 protein levels increase with 4% compared to control conditions after 1 hour of exposure,after 3 hours levels dropped to a 5% decrease compared to control conditions.

B Impact of persistent salt-induced upregulation of PIN1 or PIN3 on epidermal auxin asymmetry after 24 hours of salt-stress 2. For comparison purposes auxin asymmetry in absence of PIN1 and PIN3 regulation is also shown. Due to the lack of effect of PIN3 upregulation, control and PIN3 upregulation lines are superimposed.

C Influence of transient PIN1 upregulation on the temporal dynamics of epidermal auxin asymmetry at a distance of $590\mu m$ from the root tip. The 2 hour period of PIN1 upregulation is indicated with the grey area. PIN1 upregulation is applied both in absence and presence of an AUX/LAX pattern and feedback of auxin on AUX/LAX expression and on PIN2 membrane occupancy. For comparison purposes auxin asymmetry dynamics in absence of a transient PIN1 upregulation are also shown.

D Auxin rerouting in the presence of transient PIN1 upregulation and

auxin feedback on AUX/LAX expression and PIN2 membrane occupancy.

E A pin1 KO mutant shows a transient reduction in halotropism response after 24 hours. Seeds from a heterozygous δ pin1 parent were germinated on 0.5 MS plates and after 5 days exposed to a diagonal NaCl gradient. Seedlings that were homozygous for the pin1 tDNA insertion (-/-) showed reduced response to the NaCl gradient on both plates with a 125mM and a 200mM salt gradient compared to seedlings which were heterozygous (+/-) and seedlings which were homozygous for the wildtype (Col-0) allele (+/+). This reduction was observed after 24 hours but not after 48 hours. Two independent biological replicates were used in which 200 seedlings per treatment were quantified and genotyped. This resulted in +/- n=105, +/+ n=56 and -/- n=44 for the 0 mM treatment. For the 125 mM treatment the sample size was +/- n=122, +/+ n=120 and -/- n=59. And for 200 mM, +/- n=93, +/+ n=71 and -/- n=45.

F representative pictures of seedlings homozygous for the pin1 wildtype allele (+/+) or seedlings homozygous for the tDNA insertion (-/-) on control plates or plates with a 200 mM NaCl gradient. Coloured dots were placed at the root tip after 0 (1st black dot), 24 (green dot), 48 (blue dot) and 72 (2nd black dot) hours after applying the salt gradient. The angle from gravity after 24 hours (the angle between the line from the first to the second dot and a line straight down) is significantly smaller in the example of the -/- seedling on a 200 mM NaCl gradient as compared to the wildtype seedlings.

Supplementary Material For: Modeling halotropism: A key role for root tip architecture and reflux loop remodeling in redistributing auxin

Thea van den Berg, Ruud Korver, Christa Testerink, Kirsten ten Tusscher

1 Additional results and explanations

1.1 Auxin rerouting, different thresholds

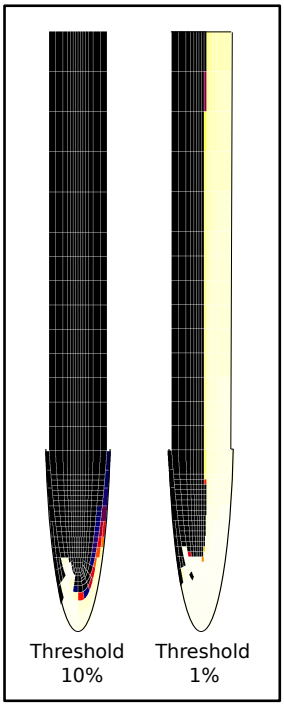

Figure S1: **Influence of measurement threshold on displayed auxin rerouting**.Auxin rerouting maps for auxin elevations of 10% or more (left) and for auxin elevatios of 1% or more (right).

Figure S1 shows two auxin rerouting maps for the same halotropism simulation. On the left, the same rerouting map is shown as in Figure 2C2 of the paper. On the right, auxin

rerouting is shown for the situation in which an auxin increase of 1% or more (rather than 10% or more) is monitored, allowing one to measure smaller amplitude auxin rerouting.

1.2 AUX/LAX influence on auxin pattern

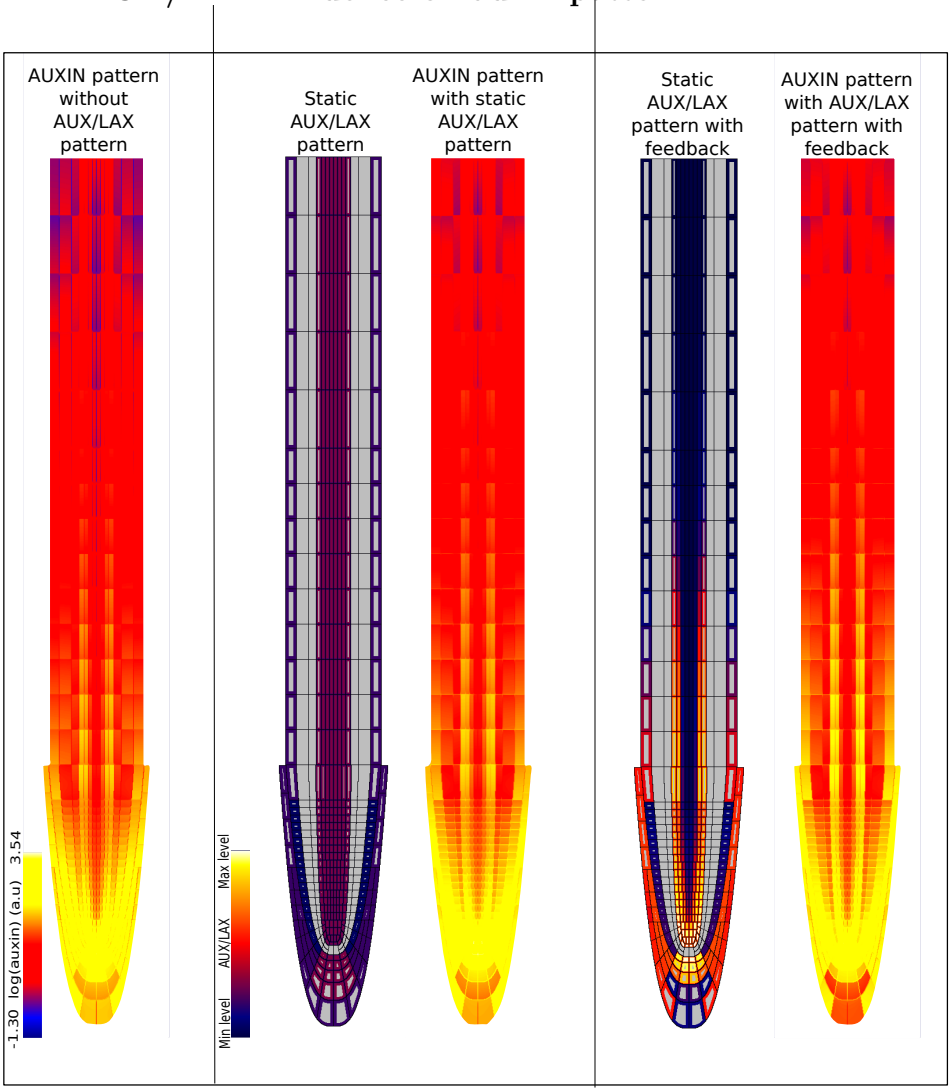

Figure S2: **Influence of AUX/LAX on root tip auxin pattern**.Left: auxin pattern in absence of AUX/LAX prepattern; Middle: AUX/LAX pattern with static AUX/LAX leves and resulting auxin pattern; Right: AUX/LAX pattern with auxin dependent AUX/LAX expression and resulting auxin pattern.

Figure S2 shows that incoroporation of a realistic AUX/LAX pattern is essential to reproduce the experimentally observed auxin patterns in which auxin levels in young, meristematic epidermal cells are low and increase upon leaving the meristem and becoming part of the elongation zone.

1.3 Auxin feedback on PIN2 membrane levels

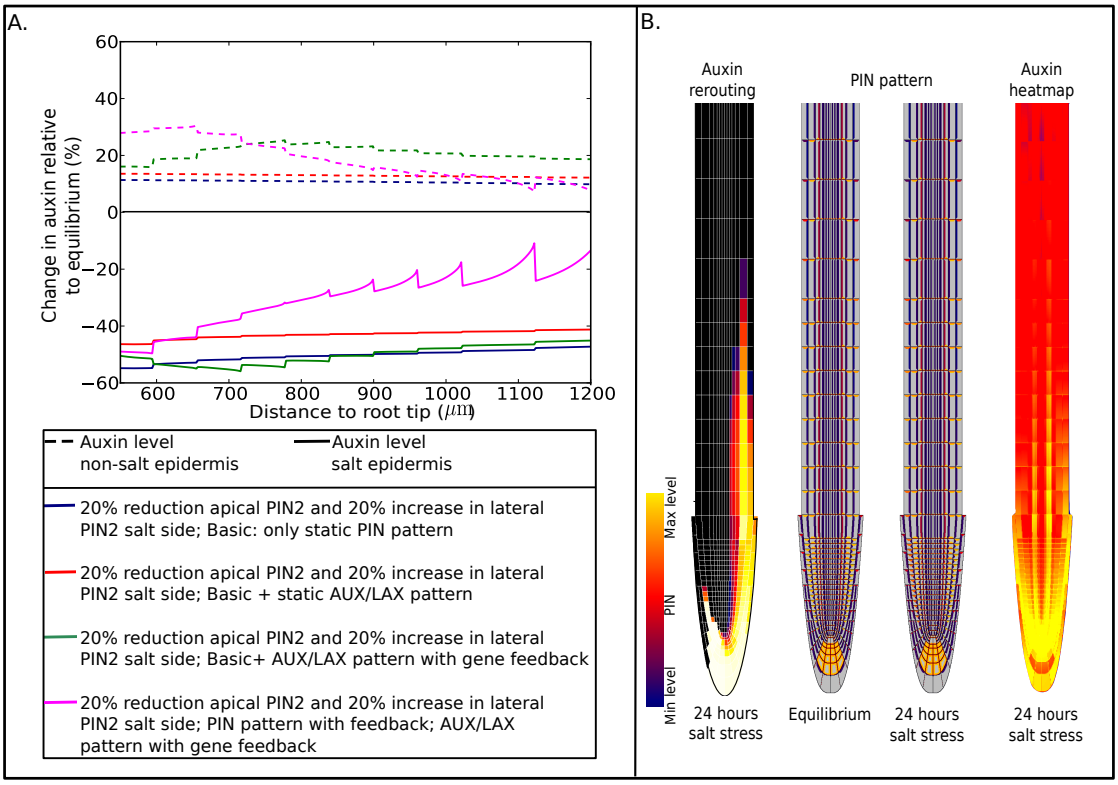

Figure S3: **Influence of auxin feedback on PIN2**. **A** Impact of auxin feedback on PIN2 on epidermal auxin assymetry after 24 hours of applying salt stress by reducing apical and increasing lateral PIN2 levels. For comparison purposes auxin asymmetry under several other conditions are also shown.**B** Auxin rerouting, change in PIN membrane occupancy pattern and resulting auxin asymmetry in presence of auxin feedback on both AUX/LAX expression and PIN2 membrane occupancy.

Figure S3 shows the effect that incorporating a positive feedback of auxin on PIN2 membrane occupancy has on auxin asymmetry generated during halotropism simulations. We can see that while auxin induced upregulation of AUX/LAX expression substantially elevated the auxin asymmetry, the added effect of auxin feedback on PIN2 appears more subtle, increasing auxin asymmetry in the lower part and reducing asymmetry in the higher parts of the elongation zone (Fig. S3). Important to consider here is that we take the PIN2 situation as observed after 6 hours of salt stress as a starting point for our simulations. As a consequence, we start our simulations from a situation in which most if not all PIN2 dynamics, directly salt induced as well as secondary auxin-feedback dependent- has most likely already taken place. In retrospect, adding auxin dependent feedback of PIN2 on top of this should not be expected to have too much effect. Indeed, auxin dependence of PIN2 might be more important for the initial establishment

of the PIN2 asymmetry.

1.4 AUX1 asymmetry under salt gradient

distance from lateral root cap (micron)	significance value
2500	0.000193054
7500	0.157423
12500	0.0118692
17500	$1.18449 * 10^{-8}$
22500	$3.61994 * 10^{-7}$
27500	$1.38665 * 10^{-8}$
32500	0.000122297
37500	$7.38984 * 10^{-9}$
42500	$3.1453 * 10^{-10}$
47500	$3.44796 * 10^{-}11$
52500	$6.1504 * 10^{-8}$
57500	0.0000609791
62500	$4.14202 * 10^{-13}$
67500	$9.73117 * 10^{-12}$
72500	$2.40387 * 10^{-20}$
77500	$9.78448 * 10^{-15}$
82500	$5.25836 * 10^{-15}$
87500	$2.01565 * 10^{-17}$
92500	$2.02167 * 10^{-14}$
97500	$1.80546 * 10^{-10}$
102500	$4.7292 * 10^{-10}$
107500	$1.61581 * 10^{-12}$
112500	$2.65674 * 10^{-10}$
117500	$2.95543 * 10^{-7}$
122500	$1.39511 * 10^{-8}$
127500	$6.17551 * 10^{-6}$
132500	0.0000357128

Table S1: Significance values for AUX1 asymmetry in salt-gradient exposed versus non exposed roots

Table S1 shows the significance values for a double sided T-test performed on AUX1 fluorescence level ratios between salt-exposed and non-salt exposed plants. Ratios were binned per 5000 micron intervals, indicated distances represent the midpoint of the bin.

1.5 PIN1 and PIN3 measurements under salt gradient

Figure S4 shows temporal dynamics of PIN1 and PIN3 levels in response to a salt gradient split out in changes occurring at basal membranes, lateral membranes, apical membranes (only for PIN3) and intracellularly. Results for the different membrane compartments and the intracellular compartment are highly similar, justifying comparison of overall (pooled) PIN1 and PIN3 levels over the course of time as shown in Figure 4 in the paper.

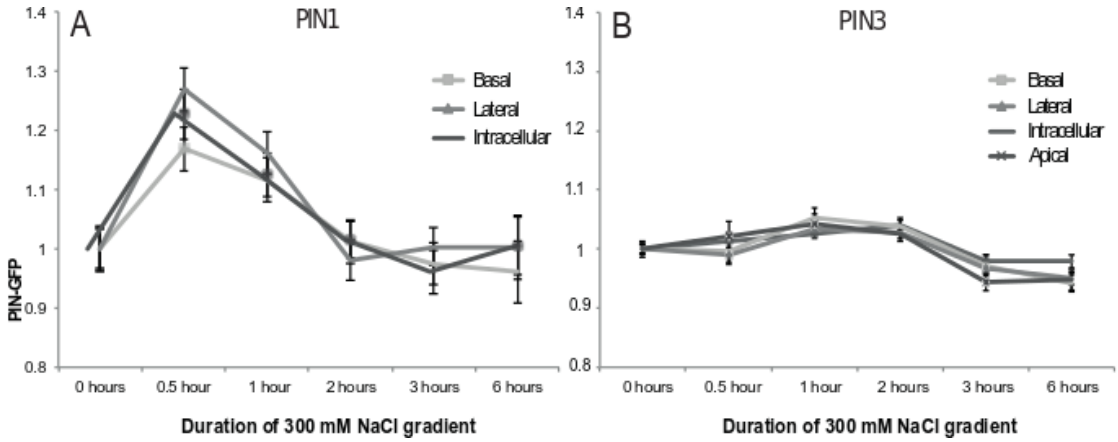

Figure S4: **PIN1 and no PIN3 re-distribution during a 300 mM NaCl gradient**. **A** PIN1-GFP and **B** PIN3-GFP intensities compared to control on the basal and lateral sides of the membrane and inside of the cell. GFP-intensities on the individual membranes and cell interior follow the same pattern as the total GFP-intensity, implying that no redistribution of PIN1 or PIN3 occurs during 6 hours of exposure to a 300mM NaCL gradient .

In our earlier work we found substantial upregulation of both PIN1 and PIN3. The differences in salt-induced upregulation of PIN1 and PIN3 found in our current and earlier experiments can be explained by differences in experimental set-up. In the Galvan-Ampudia *et al.* study roots were dipped in liquid 100 mM NaCL medium for an hour, generating a uniform and severe salt stress for the root. In contrast, in the current study roots were grown in solid medium containing a salt-gradient with a maximum of 300 mM NaCL. These conditions are more representative for naturally occurring growth conditions. Extrapolating from measurements of similar gradients in our earlier study (Galvan-Ampudia *et al.* Curr Biol 2013), we derive that salt concentrations at the tip of the root will not exceed 75 mM after 24 hours. Thus, in the current experiments roots are exposed to non-uniform and considerably lower salt-stress, explaining the reduced upregulation of PIN1 and PIN3.

1.6 Halotropism dynamics in pin1 experiment

An additional observation that can be made based on Figure 4F is that for plants with either a single or two wildtype PIN1 alleles for 125mM salt gradients angles from gravity remain constant between 24h and 48h, while for 200mM salt gradients the initial angle at 24h is larger but decreases at 48h to angles comparable to those found for 125mM. The larger initial angle under 200mM can be understood as a stronger halotropic response occuring under higher salt concentrations and is consistent with our earlier findings (Galvan-Ampudia *et al.* Curr Biol 2013). These earlier experiments also showed a takeover from halotropic by gravitropic growth around 48h of exposure to salt gradients smaller than 250mM. We hypothesize that the reduction of angles under 200mM might potentially be explained by a stronger induction of gravitropism due to the initially higher angles with gravity.

2 Model robustness

2.1 Local root tip auxin biosynthesis simula

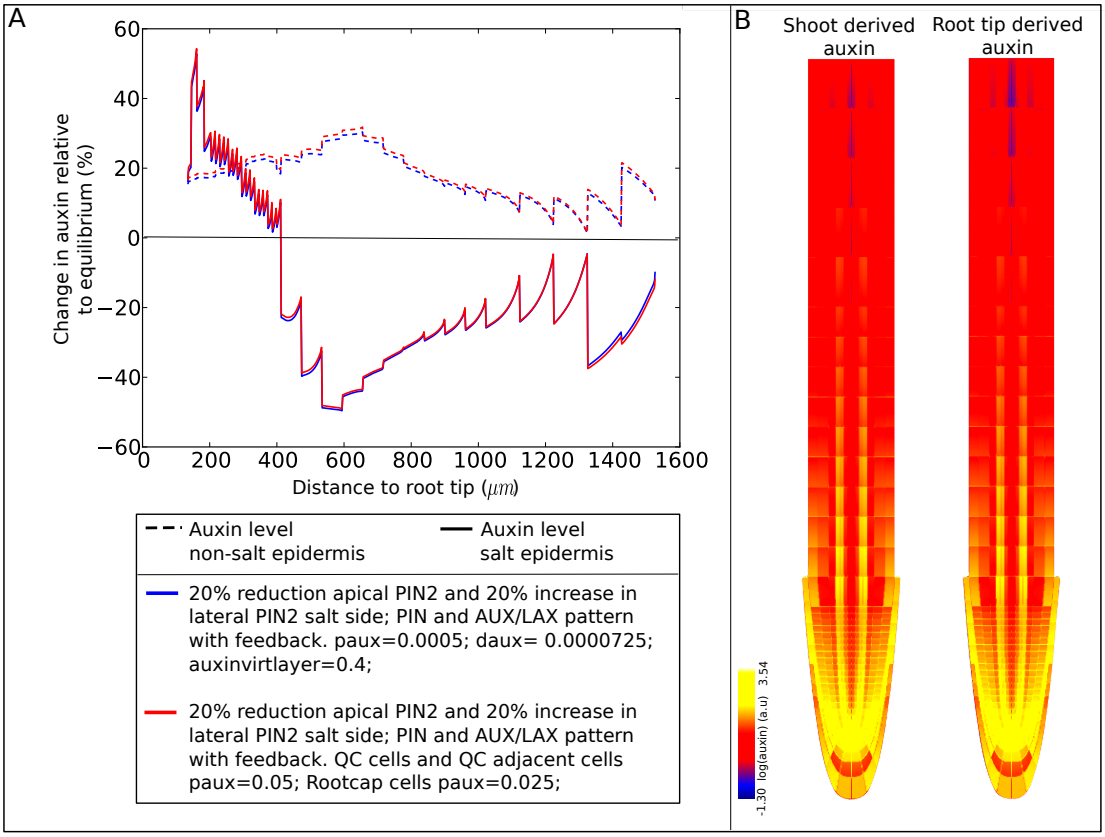

Figure S5: **Robustness to variation in location of major auxin source.** In the default model, all cells have a similar capacity to produce and degrade auxin and there is a substantial flux of auxin from the shoot. Here we reduced shoot derived auxin influx by a factor 2, while increasing auxin production in the QC by a factor 100 and in the root cap increasing auxin production a factor 50 and decreasing degradation by a factor 2. We compare the epidermal auxin asymmetry and overall auxin pattern generated during halotropism with that of the default model.

2.2 Variation of parameters

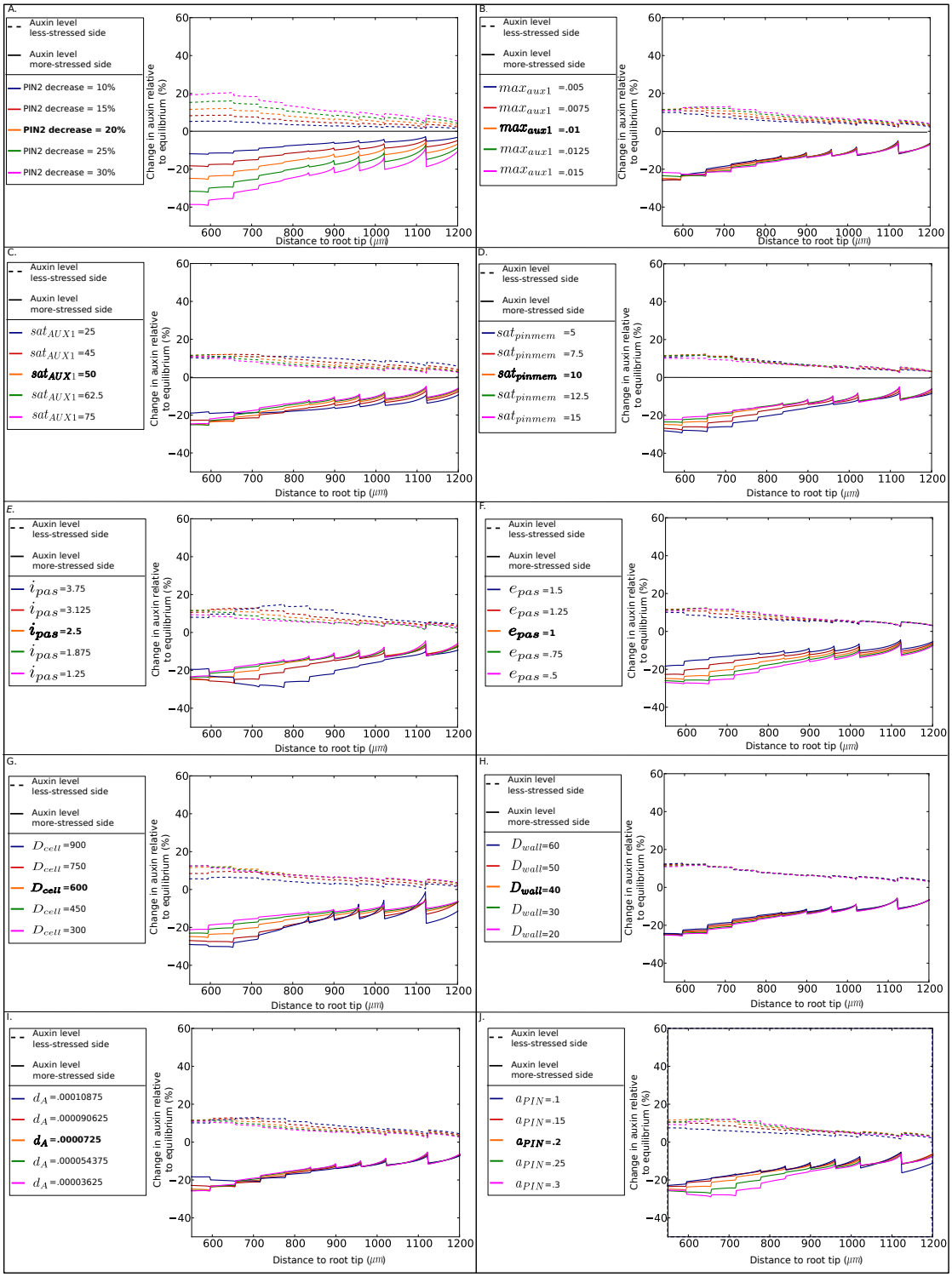

Figure S6: **Robustness to variation in parameter values.** Robustness of simulation outcomes for changes in the reduction of apical PIN2 at the salt-stressed side (**A**), changes in max_{AUX1} (**B**), changes in sat_{AUX1} (**C**), changes in sat_{pinmem} (**D**), changes in i_{pas} (**E**), changes in e_{pas} (**F**), changes in D_{cell} (**G**), changes in D_{wall} (**H**), changes in d_a (**I**) and changes in a_{PIN} (**J**). Parameter values were varied within a range of a factor 0.5 to 1.5 of the original values. All simulations were performed with the an apical PIN2 reduction of 20%, and without AUX/LAX prepattern and feedback on auxin transporters. Simulations were run for 24 hours, auxin levels during stress were compared to equilibrium levels, and plotted for the elongation zone.

Supplementary Material For: Modeling halotropism: A key role for root tip architecture and reflux loop remodeling in redistributing auxin

Thea van den Berg, Ruud Korver, Christa Testerink, Kirsten ten Tusscher

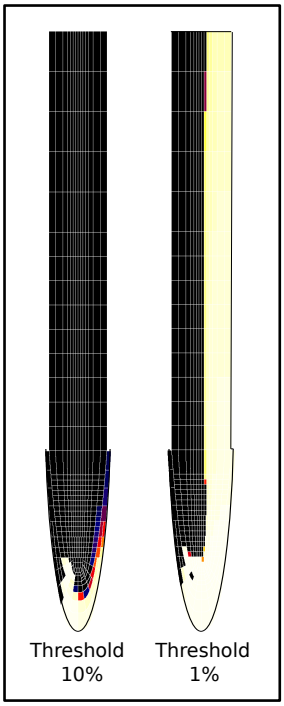

Figure S1: **Influence of measurement threshold on displayed auxin rerouting**.Auxin rerouting maps for auxin elevations of 10% or more (same as in Figure 2C, right) (left) and for auxin elevatios of 1% or more (right).

distance from lateral root cap (μm)	significance value
2.5	0.000193054
7.5	0.157423
12.5	0.0118692
17.5	$1.18449 * 10^{-8}$
22.5	$3.61994 * 10^{-7}$
27.5	$1.38665 * 10^{-8}$
32.5	0.000122297
37.5	$7.38984 * 10^{-9}$
42.5	$3.1453 * 10^{-10}$
47.5	$3.44796 * 10^{-}11$
52.5	$6.1504 * 10^{-8}$
57.5	0.0000609791
62.5	$4.14202 * 10^{-13}$
67.5	$9.73117 * 10^{-12}$
72.5	$2.40387 * 10^{-20}$
77.5	$9.78448 * 10^{-15}$
82.5	$5.25836 * 10^{-15}$
87.5	$2.01565 * 10^{-17}$
92.5	$2.02167 * 10^{-14}$
97.5	$1.80546 * 10^{-10}$
102.5	$4.7292 * 10^{-10}$
107.5	$1.61581 * 10^{-12}$
112.5	$2.65674 * 10^{-10}$
117.5	$2.95543 * 10^{-7}$
122.5	$1.39511 * 10^{-8}$
127.5	$6.17551 * 10^{-6}$
132.5	0.0000357128

Table S1: Significance values for AUX1 asymmetry in salt-gradient exposed versus non exposed roots. Significance values were computed for a double sided T-test performed on AUX1 fluorescence level ratios between salt-exposed and non-salt exposed plants. Ratios were binned per 5 μm intervals, indicated distances represent the midpoint of the bin.

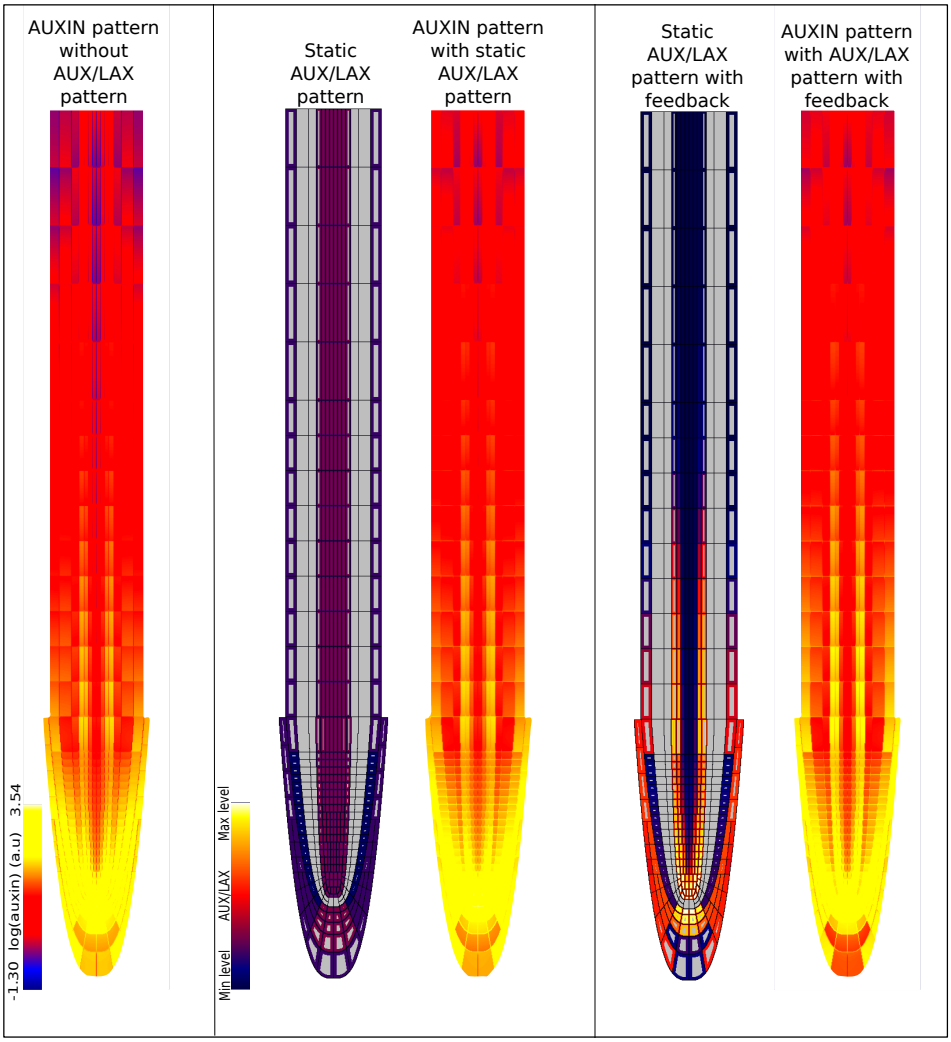

Figure S2: **Influence of AUX/LAX on root tip auxin pattern**. Left: auxin pattern in absence of AUX/LAX prepattern; Middle: AUX/LAX pattern with static AUX/LAX leves and resulting auxin pattern; Right: AUX/LAX pattern with auxin dependent AUX/LAX expression and resulting auxin pattern.

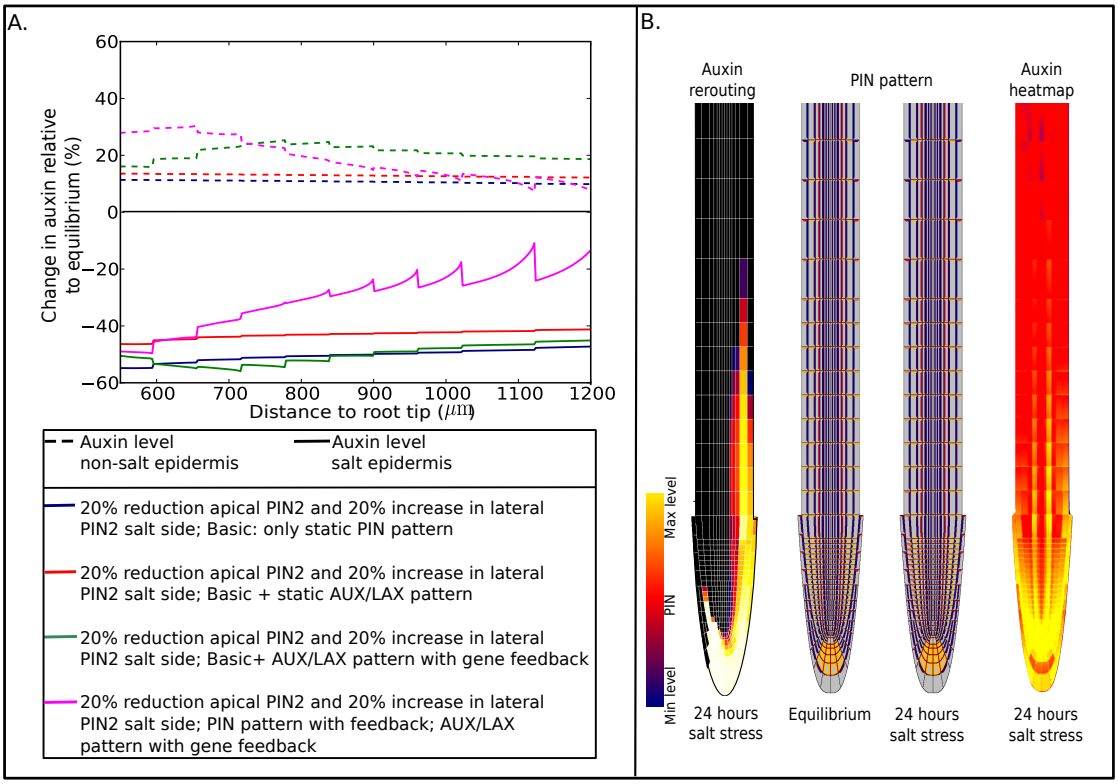

Figure S3: **Influence of auxin feedback on PIN2**. **A** Impact of positive feedback of auxin on PIN2 membrane occupancy on epidermal auxin assymetry after 24 hours of applying salt stress by reducing apical and increasing lateral PIN2 levels. For comparison purposes auxin asymmetry under several other conditions are also shown. We can see that while auxin induced upregulation of AUX/LAX expression substantially elevated the auxin asymmetry, the added effect of auxin feedback on PIN2 appears more subtle, increasing auxin asymmetry in the lower part and reducing asymmetry in the higher parts of the elongation zone. Important to consider here is that we take the PIN2 situation as observed after 6 hours of salt stress as a starting point for our simulations. As a consequence, we start our simulations from a situation in which most if not all PIN2 dynamics, directly salt induced as well as secondary auxin-feedback dependent- has most likely already taken place. In retrospect, adding auxin dependent feedback of PIN2 on top of this should not be expected to have too much effect. Indeed, auxin dependence of PIN2 might be more important for the initial establishment of the PIN2 asymmetry. **B** Auxin rerouting, change in PIN membrane occupancy pattern and resulting auxin asymmetry in presence of auxin feedback on both AUX/LAX expression and PIN2 membrane occupancy.

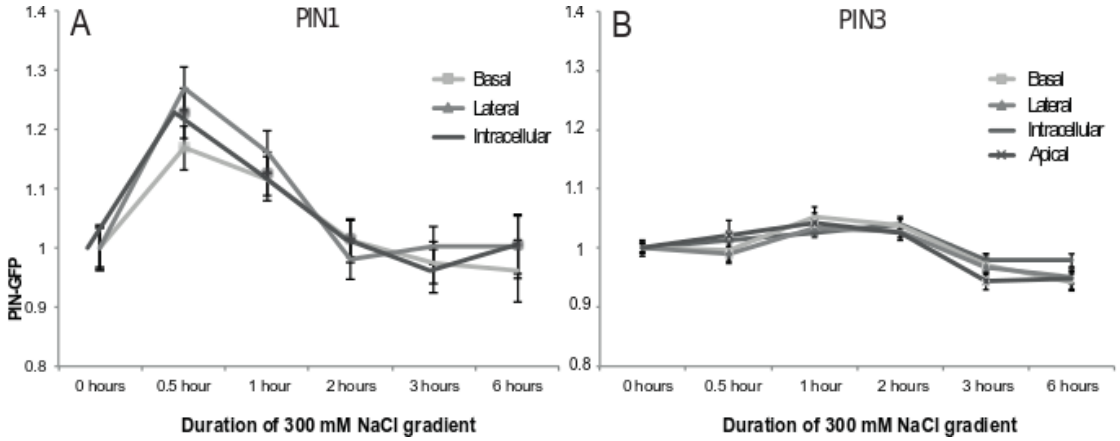

Figure S4: **PIN1 and no PIN3 re-distribution during a 300 mM NaCl gradient**. **A** PIN1-GFP and **B** PIN3-GFP intensities compared to control on the basal and lateral sides of the membrane and inside of the cell. GFP-intensities on the individual membranes and cell interior follow the same pattern as the total GFP-intensity (Fig 4), implying that no redistribution of PIN1 or PIN3 occurs during 6 hours of exposure to a 300mM NaCL gradient. Note that in our earlier work we found substantial upregulation of both PIN1 and PIN3. The differences in salt-induced upregulation of PIN1 and PIN3 found in our current and earlier experiments can be explained by differences in experimental set-up. In the Galvan-Ampudia *et al.* study roots were dipped in liquid 100 mM NaCL medium for an hour, generating a uniform and severe salt stress for the root. In contrast, in the current study roots were grown in solid medium containing a salt-gradient with a maximum of 300 mM NaCL. These conditions are more representative for naturally occurring growth conditions. Extrapolating from measurements of similar gradients in our earlier study (Galvan-Ampudia *et al.* Curr Biol 2013), we derive that salt concentrations at the tip of the root will not exceed 75 mM after 24 hours. Thus, in the current experiments roots are exposed to non-uniform and considerably lower salt-stress, explaining the reduced upregulation of PIN1 and PIN3.

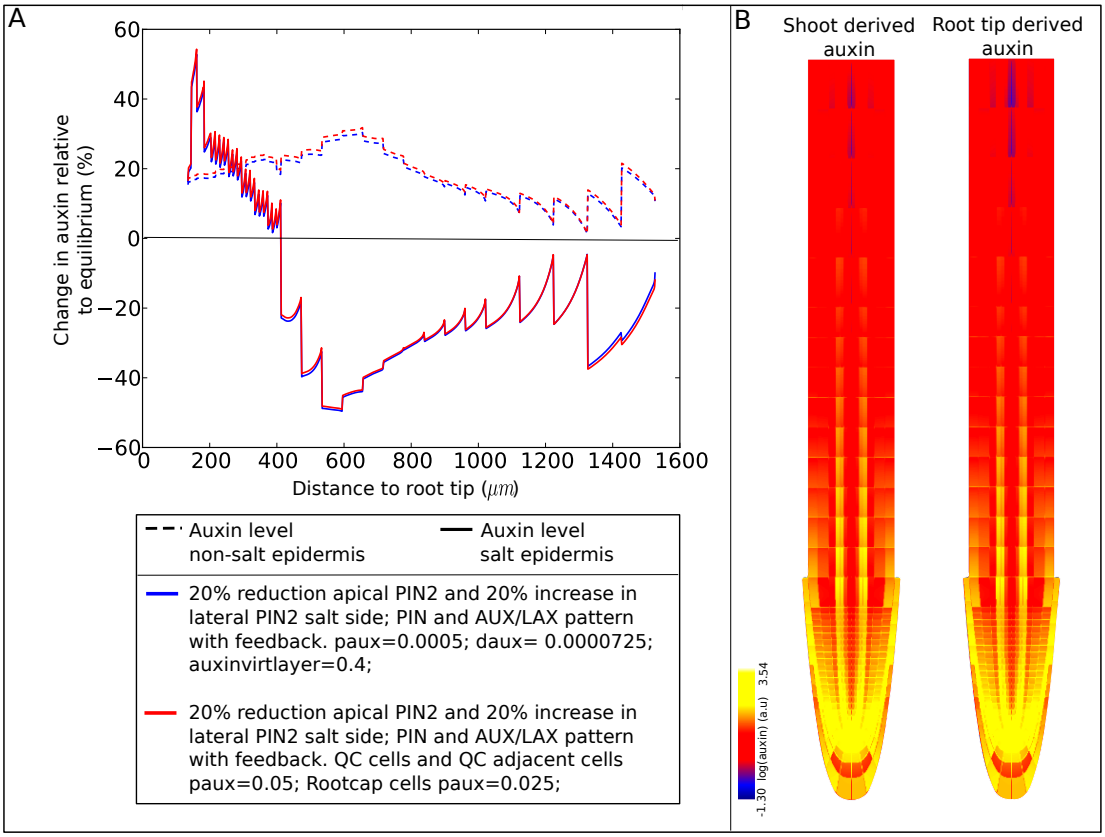

Figure S5: **Robustness to variation in location of major auxin source.** In the default model, all cells have a similar capacity to produce and degrade auxin and there is a substantial flux of auxin from the shoot. Here we reduced shoot derived auxin influx by a factor 2, while increasing auxin production in the QC by a factor 100 and in the root cap increasing auxin production a factor 50 and decreasing degradation by a factor 2. We compare the epidermal auxin asymmetry and overall auxin pattern generated during halotropism with that of the default model.

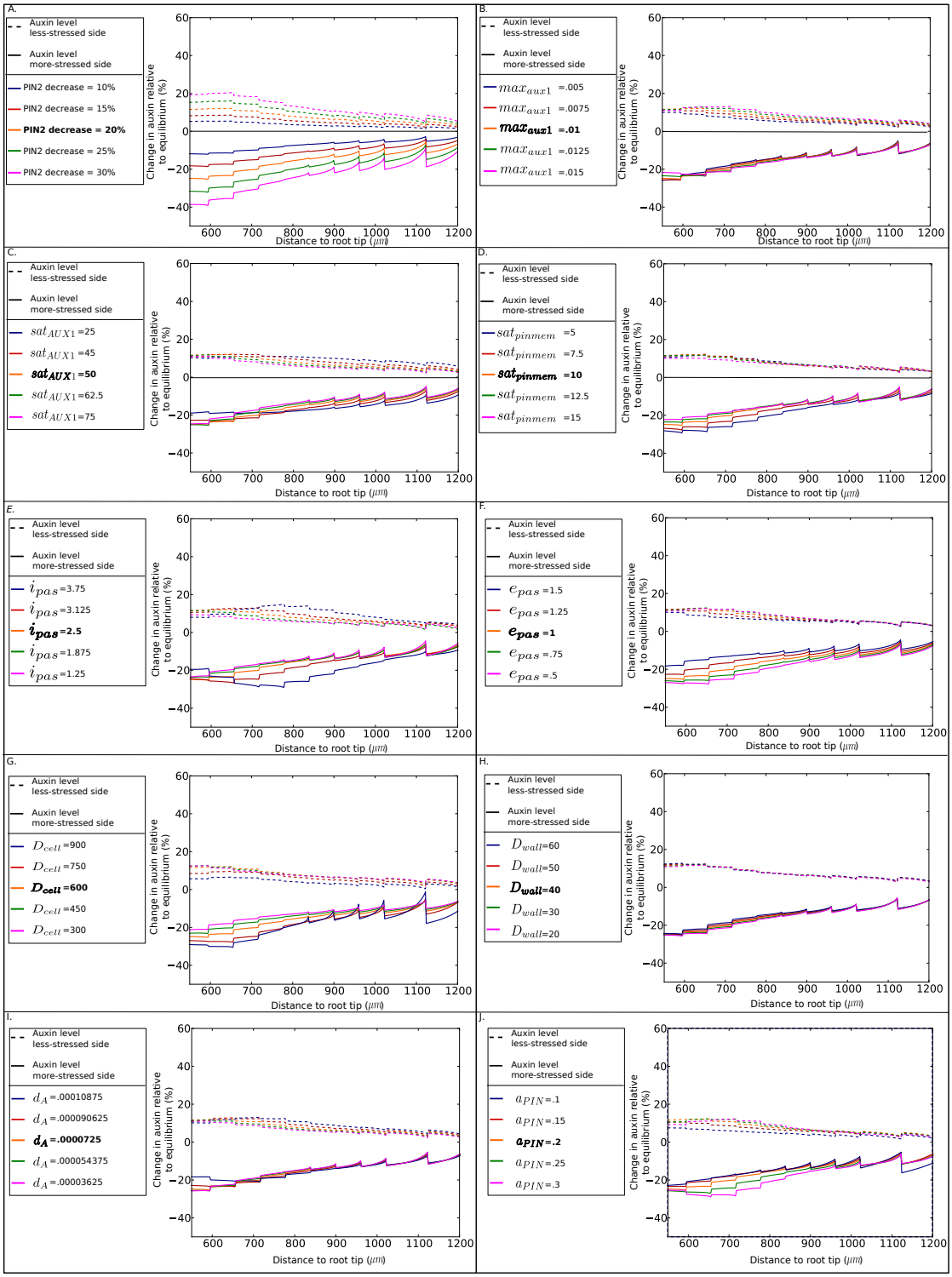

Figure S6: **Robustness to variation in parameter values.** Robustness of simulation outcomes for changes in the reduction of apical PIN2 at the salt-stressed side (**A**), changes in max_{AUX1} (**B**), changes in sat_{AUX1} (**C**), changes in sat_{pinmem} (**D**), changes in i_{pas} (**E**), changes in e_{pas} (**F**), changes in D_{cell} (**G**), changes in D_{wall} (**H**), changes in d_a (**I**) and changes in a_{PIN} (**J**). Parameter values were varied within a range of a factor 0.5 to 1.5 of the original values. All simulations were performed with the an apical PIN2 reduction of 20%, and without AUX/LAX prepattern and feedback on auxin transporters. Simulations were run for 24 hours, auxin levels during stress were compared to equilibrium levels, and plotted for the elongation zone.